JOURNAL OF GEOPHYSICAL RESEARCH, VOL. 115, B07207, doi:10.1029/2009JB006694, 2010

Low water content of the Cenozoic lithospheric mantle beneath the eastern part of the North China Craton

Qun-Ke Xia,[1] Yantao Hao,[1,2] Pei Li,[1,3] Etienne Deloule,[3] Massimo Coltorti,[2] Luigi Dallai,[4] Xiaozhi Yang,[1] and Min Feng[1]

Received 12 June 2009; revised 29 January 2010; accepted 17 February 2010; published 20 July 2010.

[1] Nominally anhydrous minerals in 46 peridotite xenoliths hosted by Cenozoic basalts from five localities (Fangshan, Penglai, Qixia, Changle, and Hebi) of the eastern part of the North China Craton (NCC) have been investigated by Fourier transform infrared spectrometry (FTIR). The water contents (H_2O wt %) of clinopyroxene (cpx), orthopyroxene (opx), and olivine (ol) range from 27 to 223 ppm, 8 to 94 ppm, and ~0 ppm, respectively. On the basis of (1) the homogenous H_2O content within single pyroxene grains and (2) the equilibrium partitioning of H_2O between cpx and opx, it is suggested that the pyroxenes largely preserve the H_2O content of their mantle source, although possible H loss during xenolith ascent cannot be excluded for ol. The recalculated whole-rock H_2O contents, using mineral modes and assuming a partition coefficient of 10 for water between cpx and ol, range from 6 to 56 ppm (average of 23 ± 13 ppm). In combination with previously reported data, the recalculated whole-rock water contents of peridotite xenoliths (105 samples from 9 localities) hosted by Cenozoic basalts from the eastern part of the NCC range from 6 to 85 ppm (average of 25 ± 18 ppm). The Cenozoic lithospheric mantle of the eastern part of the NCC is therefore characterized by a low water content compared to continental lithospheric mantle worldwide represented by typical cratonic and off-cratonic peridotites (normally 40–180 ppm, with average values of 119 ± 54 ppm and 78 ± 45, respectively) and to oceanic mantle values (>50 ppm) inferred from MORB and OIB. Peridotite xenoliths have low-to-moderate spinel $Fe^{3+}/\Sigma Fe$ (0.02–0.34) and whole rock ΔFMQ values (from −4.2 to 2.2, normally between −2.5 and 1.5), which are not correlated with pyroxene H_2O contents. Therefore, the low water contents cannot have resulted from oxidation of the mantle xenoliths and may have been caused instead by heating from an upwelling asthenosphere flow that acted in concert with NCC lithospheric thinning during the late Mesozoic to early Cenozoic. If so, the present eastern NCC lithospheric mantle represents essentially relict ancient lithospheric mantle after the thinning event, rather than newly accreted and cooled asthenospheric mantle.

Citation: Xia, Q.-K., Y. Hao, P. Li, E. Deloule, M. Coltorti, L. Dallai, X. Yang, and M. Feng (2010), Low water content of the Cenozoic lithospheric mantle beneath the eastern part of the North China Craton, *J. Geophys. Res.*, *115*, B07207, doi:10.1029/2009JB006694.

1. Introduction

[2] Although the main minerals of the lithospheric mantle (olivine, orthopyroxene, clinopyroxene, etc.) are nominally anhydrous, they still contain a significant amount of hydrogen (colloquially referred to as "water" because the contents are calculated as H_2O) [*Bell and Rossman*, 1992a]. The presence of water in mantle minerals greatly affects their physical (rheology, electrical conductivity, seismic velocity, and attenuation) and chemical (elemental diffusion, partial melting) properties and therefore those of their mantle domains [*Hirth and Kohlstedt*, 1996; *Karato and Jung*, 1998; *Hier-Majumder et al.*, 2005; *Hirschmann et al.*, 2005]. Peridotite xenoliths hosted by alkali magma are samples from the lithospheric mantle. Thus their water contents may provide information about the distribution of water in the lithospheric mantle [*Bell and Rossman*, 1992a, 1992b; *Ingrin and Skogby*, 2000; *Peslier et al.*, 2002; *Peslier and Luhr*, 2006; *Grant et al.*, 2007b; *Yang et al.*, 2008; *Li et al.*, 2008; *Bonadiman et al.*, 2009; *Peslier*, 2010].

[3] The North China Craton (NCC) is one of the major cratons in eastern Eurasia and contains crustal remnants older

[1]CAS Key Laboratory of Crust-Mantle Materials and Environments, School of Earth and Space Sciences, University of Science and Technology of China, Hefei, China.
[2]Also at Department of Earth Sciences, Ferrara University, Ferrara, Italy.
[3]Also at Centre de Recherche Pétrographiques et Géochimiques, Centre National de la Recherches Scientifique, Vandoeuvre-lés-Nancy, France.
[4]Istituto di Geoscienze e Georisorse, CNR, Pisa, Italy.

0148-0227/10/2009JB006694

Figure 1. Simplified tectonic map of eastern China showing peridotite xenolith localities. Tectonic subdivisions of the North China Craton are based on the work by *Zhao et al.* [2001].

than 3.8 Ga [*Liu et al.*, 1992]. It experienced widespread lithospheric extension since the late Mesozoic, which resulted in the removal of a large portion (>100 km in thickness) of the lithospheric mantle [*Menzies et al.*, 2007, and references therein]. Regardless of the mechanism (delamination, thermal/chemical erosion, etc.), the prerequisite of such thinning is the weakness of the lithospheric mantle. Due to the significant effects of water on mantle rheology, studying the water content and distribution in the NCC lithospheric mantle should provide pertinent information on the mechanism and process of lithospheric thinning. *Yang et al.* [2008] reported water contents of peridotite xenoliths hosted by Cenozoic basalts from Nushan and Hannuoba in the NCC, while *Bonadiman et al.* [2009] reported data from peridotite xenoliths hosted by Cenozoic basalts from Panshishan and Lianshan, which are close to Nushan. In this paper, we present the water contents of 46 peridotite xenoliths hosted by Cenozoic basalts from five localities in the NCC. Using our data and those previously published [*Yang et al.*, 2008; *Bonadiman et al.*, 2009], we will address the following questions: (1) how much water is stored in the NCC Cenozoic lithospheric mantle? (2) is there a relationship between the water content and the NCC lithospheric thinning?

2. Geological Background and the Studied Samples

2.1. Geological Background of the NCC

[4] On the basis of the lithological assemblage, tectonic evolution and P-T-t paths of metamorphic rocks, the North China Craton is divided into the Western and Eastern blocks, separated by the Trans-North China Orogenic Belt (Figure 1) [*Zhao et al.*, 2000; 2001]. The Western Block is composed of late Archean to early Proterozoic metasedimentary belts that unconformably overlie the Archean basement; the latter consists mainly of granulite facies gneiss and charnockite with small amounts of mafic granulites and amphibolites. The basement of the Trans-North China Orogen Belt consists of late Archean amphibolites and granulites, and 2.5 Ga granite-greenstone terrains. It is overlain by 2.4–2.2 Ga bimodal volcanic rocks in the southern region and thick carbonate and terrigenous sedimentary rocks interlayered with thin basalt flows in the central region. The Eastern Block is composed of late Archean orthogneisses intruded by 2.5 Ga syntectonic granitoids. The collision between the Western and Eastern blocks at 1.8–2.0 Ga ago may have led to the formation of the Trans-North China Orogenic Belt and represents the final amalgamation of the North China Craton.

[5] The North China Craton experienced a widespread tectonothermal reactivation in the Phanerozoic, marked by the emplacement of Early Paleozoic kimberlites, extensive late Mesozoic granites and intermediate to mafic intrusions, and Cenozoic basalts [*Menzies et al.*, 2007, and references therein]. Ultramafic xenoliths from the Paleozoic diamond-bearing kimberlites are highly refractory deep-seated garnet-facies peridotites. They represent a typical ancient cratonic lithospheric mantle, which was thick (~200 km) and cold (geotherm ~40 mW/m^2) at least until mid-Ordovician time [*Zheng and Lu*, 1999; *Wu et al.*, 2006; *Zhang et al.*, 2008]. In contrast, ultramafic xenoliths hosted by late Cretaceous and Cenozoic basalts are dominated by fertile spinel-facies peridotites, and represent a thin (60–100 km), hot (mean geotherm ~80 mW/m^2) and compositionally heterogeneous lithospheric mantle [*Fan and Hooper*, 1989; *Xu et al.*, 1995; *Xu et al.*, 1998; *Zheng et al.*, 1998, 2001, 2006; *Fan et al.*, 2000; *Rudnick et al.*, 2004; *Reisberg et al.*, 2005; *Ying et al.*, 2006]. These observations suggest that more than 100 km of cratonic lithosphere was removed or strongly modified during late Mesozoic-early Cenozoic time [*Menzies et al.*, 1993, 2007; *Griffin et al.*, 1998; *Xu*, 2001; *Xu et al.*, 2008; *Zheng et al.*, 2001, 2006; *Gao et al.*, 2002, 2004, 2008; *Zhang et al.*, 2002, 2008; *Zhang*, 2005, 2009; *Wu et al.*, 2003, 2006]. The mechanisms and tectonic driving forces responsible for the NCC lithospheric thinning have been intensely debated [*Menzies et al.*, 2007, and references therein].

2.2. Outcrops and Peridotite Xenoliths

[6] The investigated samples are spinel-facies peridotite xenoliths hosted by Cenozoic basalts from five localities of the eastern NCC (Figure 1). All of these xenoliths, lherzo-

litic to harzburgitic in composition, are relatively fresh and well preserved, with sizes ranging from 3 to 30 cm. A brief description of each locality and the nature of the peridotite xenoliths is provided below.

2.2.1. Fangshan

[7] Together with Panshishan and Lianshan [*Reisberg et al.*, 2005; *Bonadiman et al.*, 2009], Fangshan (GPS coordinates 32°18′59.9″N and 118°59′07.3″E) is located in the Subei basin, Jiangsu province (Figure 1). Alkali basalts from Fangshan have K-Ar ages of about 9 Ma [*Chen and Peng*, 1988]. Numerous big (up to 30 cm in diameter) and fresh peridotite xenoliths are hosted by these basalts; they are all spinel-facies peridotites, dominantly spinel lherzolites with rare spinel harzburgites. The 17 samples are coarse grained and mostly protogranular or porphyroclastic. Olivine (ol) and orthopyroxene (opx) are large (4–7 mm), while clinopyroxene (cpx) and spinel (sp) are smaller (1–3 mm). No hydrous minerals have been found.

2.2.2. Penglai

[8] Penglai volcano of Shandong province is located in the northeast part of Shandong Peninsula (Figure 1). Xenoliths occur in alkali basalts with 8 Ma K-Ar ages [*Liu et al.*, 1990]. A set of coarse-grained spinel lherzolites from this locality (GPS coordinates of the outcrop are 37°46′42.2″N and 120°44′46.4″E) has been investigated. No hydrous minerals were found in Penglai xenoliths.

2.2.3. Qixia

[9] The Qixia volcano is located in Shandong province about 50 km south of Penglai (GPS coordinates 37°12′15.5″N and 120°43′23.8″E) (Figure 1). Six spinel lherzolites with coarse-grained or fine-grained textures hosted by ~6 Ma olivine nephelinites [*Liu et al.*, 1990] were collected. No hydrous minerals have been found in these peridotites.

2.2.4. Changle

[10] The Changle volcano erupted in Shandong province, in the proximity of the Tan-Lu fault (Figure 1). Peridotite and websterite xenoliths and pyroxene and corundum megacrysts are found mainly in the 18–16 Ma and 10–9 Ma alkali basalts [*Jin*, 1985]. Five anhydrous, coarse-grained spinel lherzolites and one spinel harzburgite were investigated. The outcrop GPS coordinates are 36°37′11.5″N and 118°51′59.3″E.

2.2.5. Hebi

[11] The Hebi volcano (GPS coordinates 35°47′10.1″N and 114°12′34.7″E) of Henan province erupted ~4 Myr ago [*Liu et al.*, 1990]. Olivine nephelinites contain abundant small mantle xenoliths (1–5 cm in diameter) and garnet and pyroxene megacrysts. Hebi xenoliths are mainly refractory harzburgites with minor spinel lherzolites [*Zheng et al.*, 2001]. On the basis of major element compositions and in situ sulfide Re-Os isotope analysis of harzburgite xenoliths [*Zheng et al.*, 2001, 2006], Hebi is the only locality in the NCC with evidence of Archean relict mantle. All of the nine xenoliths studied are spinel harzburgites except for HB64, which is a spinel lherzolite.

3. Analytical Methods

3.1. Electron Microprobe

[12] The mineral compositions were determined using a JEOL Superprobe (JXA 8100) electron microprobe (EMP) at Nanjing University, China, with the following operating conditions: 15 kV accelerating voltage, 10 nA beam current and <5 μm beam diameter. Natural minerals and synthetic oxides were used as standards, and a program based on the ZAF procedure was used for data correction. Multipoint measurements were carried out from the core to the rim of each mineral grain, and three to four grains of each mineral were measured in each sample.

3.2. Micro-FTIR

[13] Double-polished thin sections with a thickness ranging from 0.2 to 0.4 mm were prepared for FTIR analysis. Unpolarized spectra were obtained from 1000 to 5000 cm^{-1} on a Nicolet 5700 FTIR spectrometer coupled with a Continuμm microscope at the University of Science and Technology of China (USTC), using a KBr beam splitter and a liquid-nitrogen cooled MCT-A detector. For cpx and opx, a total of 128 or 256 scans were accumulated for each spectrum at a 2 or 4 cm^{-1} resolution; for olivine up to 600 scans were accumulated. The aperture size was set from 30 × 30 to 100 × 100 μm, depending on the size and quality of the mineral grains. Measurements were made through optically clean, inclusion- and crack-free areas (usually the core region of selected grains) under a continuous dry N_2 gas flush.

[14] A modified form of the Beer-Lambert law was used to calculate the water content:

$$c = \Delta/(I \times t \times \gamma)$$

where c is the content of hydrogen species (ppm H_2O wt %), Δ is the integrated area (cm^{-2}) of absorption bands in the region of interest, I is the integral specific absorption coefficient (ppm^{-1} cm^{-2}), t is thickness (cm), and γ is the orientation factor discussed by *Paterson* [1982]. OH absorption bands were integrated between 3000 and 3800 cm^{-1} for cpx and 2800 to 3800 cm^{-1} for opx to obtain Δ values; the integral specific coefficient of 7.09 ppm^{-1} cm^{-2} for cpx and of 14.84 ppm^{-1} cm^{-2} for opx were used [*Bell et al.*, 1995] to calculate H_2O content; thickness was measured using a digital micrometer and reported as the average of 30–40 measurements covering the whole section; an orientation factor of 1/3 was used in the calculation for cpx and opx [*Paterson*, 1982]. Baseline corrections were carried out by hand at least three times for each spectrum, the uncertainty was less than 5% and the average corrected spectrum was used to calculate water content. To minimize possible uncertainties from the unpolarized determination of these optically anisotropic minerals, more than 15–20 different grains of each mineral (more than 25 grains for ol) in the same sample were analyzed, and the average value was used to define the water content of that mineral in that sample [*Asimow et al.*, 2006; *Grant et al.*, 2007b; *Kovacs et al.*, 2008]. Uncertainties in the calculated water contents come from (1) using unpolarized infrared beams on unoriented minerals (<10%); (2) baseline correction (<5%); (3) variable sample thickness (<3%); and (4) differences between the absorption coefficients (<10%) of our samples and those of samples used by *Bell et al.* [1995] due to differences in composition. The total uncertainty is estimated to be less than 20–30%.

[15] Detailed FTIR profile analysis performed at the USTC lab of two augite megacrysts hosted by Nushan Cenozoic basanites confirmed the homogeneity of their water contents. These were used as standards to detect potential

Table 1. Major Element Concentrations of Olivines From Peridotite Xenoliths Hosted by Cenozoic Basalts of the Eastern NCC[a]

Sample	SiO_2	TiO_2	Al_2O_3	Cr_2O_3	FeO	MnO	MgO	CaO	Na_2O	K_2O	NiO	TOTAL	Mg #
Panshishan													
PSS01	42.05	0.02	0.00	0.00	9.83	0.14	49.32	0.03	0.00	0.01	0.33	101.75	89.94
PSS02	41.80	0.03	0.00	0.03	10.04	0.12	49.28	0.04	0.01	0.00	0.47	101.82	89.75
PSS05	41.07	0.00	0.02	0.01	9.55	0.13	48.82	0.03	0.01	0.00	0.21	99.85	90.11
PSS07	40.82	0.00	0.00	0.01	10.40	0.14	49.42	0.02	0.01	0.01	0.30	101.13	89.45
PSS10	40.75	0.00	0.00	0.01	9.43	0.13	49.58	0.03	0.01	0.00	0.32	100.28	90.36
PSS11	40.77	0.00	0.01	0.01	9.54	0.16	50.24	0.03	0.00	0.01	0.39	101.16	90.38
PSS12	40.97	0.01	0.00	0.02	9.95	0.18	48.80	0.04	0.00	0.00	0.22	100.18	89.74
PSS13	40.97	0.00	0.00	0.00	9.24	0.13	49.69	0.03	0.01	0.01	0.32	100.40	90.55
PSS15	40.54	0.01	0.01	0.01	9.64	0.16	50.04	0.04	0.00		0.39	100.82	90.25
PSS16	40.57	0.00	0.02	0.01	10.04	0.16	48.79	0.05	0.00	0.00	0.29	99.93	89.66
PSS17	41.94	0.01	0.01	0.04	9.27	0.13	50.02	0.04	0.00	0.01	0.43	101.92	90.58
PSS18	41.03	0.00	0.00	0.02	9.37	0.16	48.99	0.02	0.00	0.00	0.25	99.85	90.31
PSS19	40.93	0.01	0.01	0.01	9.80	0.13	49.63	0.01	0.01	0.01	0.33	100.86	90.03
PSS20	40.74	0.00	0.00	0.02	9.81	0.14	50.05	0.03	0.01	0.00	0.37	101.18	90.09
Lianshan													
LS01	40.62	0.01	0.01	0.00	9.61	0.13	49.05	0.02	0.01	0.00	0.32	99.77	90.10
LS02	40.81	0.01	0.01	0.01	9.75	0.13	49.15	0.03	0.01	0.00	0.31	100.22	89.99
LS03	42.16	0.01	0.01	0.01	8.36	0.12	50.32	0.05	0.01	0.01	0.41	101.48	91.47
LS04	40.79	0.00	0.02	0.01	10.18	0.17	48.98	0.04	0.01	0.00	0.28	100.49	89.56
LS05	39.86	0.01	0.01	0.01	9.48	0.14	49.93	0.03	0.02		0.38	99.85	90.38
LS06	40.74	0.00	0.01	0.02	9.83	0.13	48.79	0.04	0.00	0.00	0.31	99.87	89.85
LS07	40.86	0.00	0.01	0.01	9.78	0.13	49.20	0.05	0.01	0.00	0.31	100.37	89.97
LS08	41.04	0.00	0.00	0.00	9.68	0.14	49.57	0.03	0.01	0.01	0.31	100.79	90.13
LS12	40.69	0.01	0.00	0.01	8.16	0.14	50.98	0.05	0.00		0.42	100.46	91.76
LS17	40.89	0.01	0.01	0.01	8.21	0.14	51.20	0.04	0.00		0.39	100.90	91.75
LS19	40.67	0.01	0.01	0.00	9.32	0.12	49.89	0.02	0.00	0.00	0.31	100.36	90.52
LS20	41.96	0.03	0.00	0.03	9.49	0.14	49.73	0.04	0.00	0.00	0.38	101.80	90.33
LS21	40.89	0.00	0.00	0.01	8.20	0.12	49.50	0.02	0.02	0.01	0.29	99.06	91.50
LS22	40.52	0.01	0.01	0.01	10.44	0.14	48.51	0.04	0.01	0.01	0.29	99.99	89.23
LS23	41.89	0.01	0.01	0.06	10.04	0.13	49.13	0.02	0.01	0.03	0.36	101.69	89.71
LS24	40.84	0.01	0.00	0.00	9.86	0.12	49.20	0.04	0.01	0.00	0.28	100.37	89.89
LS26	40.89	0.01	0.01	0.02	8.96	0.12	50.38	0.03	0.01	0.00	0.34	100.76	90.93
LS30	40.67	0.01	0.01	0.02	9.69	0.14	48.04	0.05	0.00	0.00	0.31	98.94	89.84
LS31	40.76	0.00	0.00	0.00	10.35	0.13	48.55	0.02	0.01	0.00	0.34	100.15	89.32
Fangshan													
FS01	40.99	0.01	0.02	0.03	9.03	0.16	49.18	0.06	0.01	0.01	0.23	99.73	90.66
FS03	41.08	0.00	0.05	0.04	8.69	0.11	49.49	0.13	0.01	0.00	0.24	99.84	91.04
FS06	40.89	0.01	0.01	0.01	8.84	0.14	49.26	0.05	0.01	0.01	0.23	99.45	90.86
FS07	40.47	0.00	0.01	0.01	9.82	0.15	48.71	0.08	0.01	0.00	0.23	99.50	89.84
FS11	40.57	0.01	0.01	0.01	9.21	0.13	50.32	0.12	0.04		0.39	100.82	90.69
FS12	41.22	0.01	0.03	0.02	9.18	0.14	48.57	0.10	0.02	0.00	0.24	99.53	90.42
FS13	40.95	0.02	0.04	0.03	9.69	0.15	48.88	0.09	0.01	0.00	0.24	100.08	90.00
FS14	40.91	0.01	0.04	0.02	9.73	0.13	48.55	0.07	0.02	0.01	0.21	99.70	89.89
FS16	41.30	0.00	0.02	0.01	8.72	0.14	49.46	0.06	0.01	0.00	0.24	99.98	91.00
FS17	40.87	0.00	0.02	0.02	8.88	0.16	48.95	0.05	0.03	0.01	0.26	99.24	90.77
FS18	40.09	0.02	0.04	0.04	10.07	0.15	49.52	0.12	0.00		0.36	100.42	89.76
FS19	40.94	0.01	0.04	0.01	9.68	0.14	48.70	0.10	0.01	0.01	0.23	99.85	89.97
FS21	40.93	0.01	0.03	0.02	9.80	0.14	48.51	0.05	0.02	0.00	0.25	99.76	89.82
FS23	41.15	0.00	0.02	0.04	9.00	0.12	48.98	0.08	0.01	0.01	0.24	99.66	90.65
FS24	40.48	0.00	0.01	0.01	8.82	0.14	50.61	0.04	0.00		0.43	100.56	91.09
FS26	40.84	0.00	0.01	0.02	9.89	0.14	48.40	0.04	0.00	0.00	0.23	99.58	89.72
Penglai													
PL01	41.08	0.02	0.02	0.00	9.87	0.15	49.19	0.02	0.00	0.00	0.28	100.64	89.89
PL10	41.14	0.01	0.01	0.02	9.52	0.15	48.90	0.04	0.01	0.00	0.27	100.08	90.16
PL17	41.13	0.01	0.01	0.01	9.75	0.17	48.66	0.03	0.01	0.00	0.27	100.05	89.89
PL19	41.26	0.01	0.03	0.01	9.89	0.14	48.89	0.03	0.01	0.00	0.29	100.55	89.81
PL32	41.08	0.00	0.01	0.00	9.90	0.18	48.46	0.03	0.00	0.01	0.26	99.94	89.72
PL36	41.07	0.01	0.01	0.00	9.86	0.10	49.01	0.02	0.01	0.00	0.22	100.32	89.86
PL42	41.09	0.02	0.01	0.01	9.47	0.14	49.50	0.04	0.01	0.01	0.28	100.60	90.31
PL44	40.86	0.01	0.00	0.01	10.27	0.17	48.77	0.04	0.00	0.00	0.30	100.42	89.43
PL46	41.14	0.00	0.01	0.02	8.56	0.12	50.43	0.03	0.00	0.01	0.29	100.61	91.31
Changle													
CL22	41.29	0.00	0.03	0.03	10.89	0.17	47.78	0.04	0.00	0.01	0.24	100.46	88.67
CL31	41.00	0.00	0.02	0.00	9.87	0.18	48.51	0.03	0.02	0.00	0.28	99.91	89.75
CL32	40.85	0.00	0.00	0.03	10.33	0.17	48.41	0.01	0.00	0.01	0.24	100.04	89.31
CL35	41.07	0.02	0.02	0.03	9.33	0.12	49.31	0.05	0.01	0.00	0.25	100.20	90.41
CL38	41.11	0.03	0.01	0.04	9.99	0.17	49.22	0.02	0.00	0.00	0.25	100.84	89.78

Table 1. (continued)

Sample	SiO_2	TiO_2	Al_2O_3	Cr_2O_3	FeO	MnO	MgO	CaO	Na_2O	K_2O	NiO	TOTAL	Mg #
							Qixia						
QX01	41.24	0.01	0.00	0.00	8.59	0.13	50.00	0.02	0.00	0.00	0.24	100.23	91.21
QX04	41.14	0.00	0.01	0.00	8.66	0.19	49.35	0.00	0.02	0.00	0.27	99.64	91.04
QX14	41.34	0.00	0.00	0.02	9.05	0.13	48.83	0.01	0.00	0.00	0.23	99.62	90.58
QX18	41.25	0.00	0.01	0.00	8.42	0.10	49.06	0.03	0.01	0.00	0.23	99.11	91.22
QX49	41.32	0.00	0.02	0.00	8.87	0.19	48.40	0.00	0.01	0.00	0.20	99.01	90.68
QX50	41.36	0.00	0.01	0.02	8.52	0.14	49.47	0.02	0.00	0.00	0.24	99.77	91.19
QX51	41.18	0.00	0.00	0.01	8.29	0.14	49.64	0.01	0.00	0.01	0.22	99.50	91.44
							Hebi						
HB01	41.57	0.01	0.01	0.02	7.81	0.11	49.81	0.07	0.01	0.00	0.26	99.68	91.91
HB02	41.41	0.01	0.01	0.01	7.91	0.13	50.13	0.04	0.01	0.00	0.25	99.92	91.87
HB06	41.76	0.02	0.01	0.00	7.33	0.11	50.20	0.06	0.00	0.00	0.26	99.78	92.43
HB07	41.52	0.01	0.01	0.01	7.82	0.12	50.29	0.02	0.01	0.00	0.26	100.07	91.98
HB10	41.50	0.00	0.01	0.02	7.17	0.09	51.03	0.01	0.00	0.00	0.27	100.12	92.70
HB12	41.62	0.00	0.03	0.04	7.16	0.14	50.74	0.07	0.00	0.00	0.29	100.09	92.67
HB16	41.28	0.00	0.02	0.03	7.70	0.13	50.11	0.08	0.00	0.00	0.30	99.66	92.07
HB17	41.63	0.00	0.02	0.02	7.21	0.11	50.24	0.07	0.02	0.00	0.24	99.58	92.55
HB64	40.73	0.00	0.02	0.00	11.50	0.17	46.88	0.06	0.02	0.00	0.18	99.56	87.91

[a]Mg # = 100 Mg/(Mg + Fe). Panshishan and Lianshan samples are also included because no olivine data have been given by *Bonadiman et al.* [2009].

instrument drift during analysis. During the analytical period including all of the NCC peridotites, the maximum variation for the two augites was <4% both for peak height and integrated area within the OH absorption area. The augites were also analyzed at the LMTG lab (Toulouse, France). The maximum difference of peak height and integrated area within the OH absorption area between the USTC and the LMTG labs was <3% during these crosscheck analyses.

4. Results

4.1. Mineral Chemistry and Thermometry

[16] The EMP analyses demonstrate the chemical homogeneity of the samples, with no variations observed among different grains of the same mineral of a given sample. The average values for ol, cpx, opx and sp. are reported in Tables 1–4. Our results are similar to the previously reported data for these localities [*Fan and Hooper*, 1989; *Zheng et al.*, 1998, 2001; *Rudnick et al.*, 2004]. Mg numbers (Mg # = 100 Mg/(Mg + Fe)) of ol from Fangshan, Penglai, Changle, and Qixia range between 88.7 and 91.2, typical for off-craton spinel peridotite xenoliths [*Gaul et al.*, 2000] and lower than those of cratonic peridotites (typically >92 with an average of 92.8 [*Bernstein et al.*, 2007]). The Hebi harzburgites are highly refractory with Mg # of ol ranging between 91.9 and 92.7, similar to those reported by *Zheng et al.* [2001]. One spinel lherzolite (HB64) is relatively fertile, with an ol Mg # of 87.9.

[17] Both experimental studies [e.g., *Jaques and Green*, 1980] and natural samples [e.g., *Arai*, 1994] show that Mg # of ol and Cr # (= 100Cr/(Cr + Al)) of sp. progressively increase in peridotite residues with increasing melt extraction. With the exception of sample HB64 from Hebi, Mg # of ol and Cr # of sp. of our samples define a positive trend (Figure 2), suggesting a partial melting process.

[18] Equilibrium temperatures are estimated using the Ca-in-opx geothermometer of *Brey and Kohler* [1990] at a pressure of 15 kbar (Table 5). These temperatures vary between 900 and 1150°C, in the range of those previously reported for the NCC peridotites [*Fan and Hooper*, 1989; *Xu et al.*, 1995; *Zheng et al.*, 1998, 2001, 2006; *Chen et al.*, 2001; *Rudnick et al.*, 2004; *Xu and Bodinier*, 2004].

4.2. Hydrogen Species and Water Content

[19] All the analyzed pyroxene grains in these peridotite xenoliths exhibit several prominent absorption bands in the OH-stretching vibration region (3000–3800 cm^{-1}). Representative infrared spectra are shown in Figure 3a for cpx and Figure 3b for opx. In contrast, most of the coexisting ol have no detectable OH peak; only a few grains from Fangshan and Changle display weak OH bands (Figure 3c).

[20] The IR absorption bands of pyroxenes can be divided into different groups: (1) cpx: 3600–3635 cm^{-1}, 3510–3550 cm^{-1}, 3445–3470 cm^{-1}; and (2) opx: 3570–3595 cm^{-1}, 3500–3525 cm^{-1}, 3390–3415 cm^{-1}, 3300–3315 cm^{-1}. The positions of these absorption bands are similar to those reported in earlier studies, and interpreted as resulting from the vibration of structural OH [*Skogby and Rossman*, 1989; *Skogby et al.*, 1990; *Bell and Rossman*, 1992a; *Ingrin and Skogby*, 2000; *Peslier et al.*, 2002; *Grant et al.*, 2007b; *Yang et al.*, 2008; *Li et al.*, 2008; *Bonadiman et al.*, 2009; *Gose et al.*, 2009b]. The relative absorbancy of these bands varies among grains in a given sample due to their variable orientation of grains with respect to the IR beam direction. Hydrogen profile measurements performed on the larger pyroxene grains in each suite of samples show no obvious variations between core and rim regions (Figure 3d). For ol grains with weak OH absorption bands (Figure 3c), the main peaks are at 3572 cm^{-1} and 3525 cm^{-1}, typical of mantle olivine [*Bell and Rossman*, 1992a; *Berry et al.*, 2005; *Demouchy et al.*, 2006; *Peslier and Luhr*, 2006; *Grant et al.*, 2007b; *Li et al.*, 2008].

[21] The water contents (ppm H_2O, wt %) measured in pyroxene are given in Table 5. H_2O contents vary from 27 to 223 ppm for cpx (Fangshan, 41–177 ppm; Penglai, 27–59 ppm; Qixia, 70–158 ppm; Changle, 71–223 ppm; Hebei, 181 ppm) and from 8 to 94 ppm for opx (Fangshan, 21–74 ppm; Penglai, 8–25 ppm; Qixia, 32–59 ppm; Changle,

Table 2. Major Element Concentrations of Clinopyroxenes From Peridotite Xenoliths Hosted by Cenozoic Basalts of the Eastern NCC[a]

Sample	SiO_2	TiO_2	Al_2O_3	Cr_2O_3	FeO	MnO	MgO	CaO	Na_2O	K_2O	NiO	TOTAL	Mg #
Panshishan													
PSS01	53.14	0.58	6.53	0.85	2.57	0.06	15.14	20.37	1.57	0.01	0.05	100.87	91.32
PSS02	53.26	0.45	6.43	0.91	2.61	0.07	15.06	20.21	1.69	0.00	0.07	100.76	91.15
PSS05	52.44	0.41	6.94	0.85	2.47	0.09	14.77	20.17	1.62	0.00	0.01	99.78	92.36
PSS07	52.26	0.55	6.67	0.56	2.46	0.08	14.43	21.02	1.87	0.01	0.04	99.94	91.28
PSS10	52.20	0.53	4.55	0.88	2.29	0.08	15.81	22.13	1.07	0.00	0.05	99.59	92.49
PSS11	52.26	0.58	6.42	0.86	2.45	0.07	15.10	21.33	1.76	0.00	0.05	100.87	91.65
PSS12	51.89	0.57	6.77	0.73	2.62	0.11	14.88	20.38	1.58	0.01	0.01	99.53	92.36
PSS13	52.38	0.28	5.05	0.88	2.26	0.08	15.52	21.76	1.25	0.00	0.04	99.50	92.46
PSS15	52.23	0.62	6.16	0.82	2.41	0.08	15.28	21.71	1.65	0.00	0.04	101.00	91.89
PSS16	53.77	0.61	6.96	0.63	3.08	0.09	14.20	19.59	1.74	0.01	0.05	100.72	89.17
PSS17	53.41	0.21	4.23	1.05	2.25	0.07	16.33	22.30	0.85	0.00	0.03	100.75	92.84
PSS18	52.59	0.56	4.91	0.41	2.21	0.07	15.30	22.45	0.89	0.01	0.02	99.39	92.36
PSS19	52.42	0.31	7.48	0.69	2.04	0.09	13.83	20.79	2.19	0.01	0.03	99.87	92.36
PSS20	52.02	0.65	5.30	0.89	2.29	0.07	15.70	22.63	1.20	0.01	0.04	100.80	92.45
Lianshan													
LS01	51.87	0.47	5.74	0.74	2.44	0.07	14.76	21.09	1.60	0.01	0.03	98.82	91.51
LS02	52.32	0.51	6.58	0.84	2.55	0.07	14.82	20.94	1.77	0.01	0.04	100.44	91.20
LS03	54.29	0.11	3.87	1.11	2.24	0.09	16.22	21.82	1.14	0.00	0.06	100.96	92.82
LS04	51.76	0.63	7.01	0.76	2.90	0.08	14.72	20.03	1.76	0.01	0.02	99.67	90.04
LS05	51.80	0.48	6.58	0.81	2.41	0.09	14.79	21.23	1.88	0.01	0.04	100.10	91.62
LS06	51.79	0.52	6.40	0.92	2.52	0.08	14.84	20.29	1.69	0.00	0.05	99.10	91.31
LS07	51.91	0.52	6.39	0.77	2.64	0.09	14.96	20.37	1.67	0.00	0.03	99.36	91.00
LS08	52.48	0.43	5.81	0.61	2.31	0.08	14.82	20.74	1.77	0.01	0.04	99.11	91.96
LS12	53.03	0.14	4.04	0.97	2.27	0.09	16.76	22.37	0.98	0.00	0.04	100.68	92.94
LS17	54.06	0.04	3.36	1.16	2.11	0.07	16.94	22.25	1.22	0.00	0.02	101.23	93.46
LS19	52.79	0.22	4.36	1.29	2.18	0.07	15.56	21.52	1.43	0.01	0.04	99.46	92.72
LS20	53.97	0.30	5.59	1.28	2.61	0.11	15.42	20.24	1.77	0.01	0.05	101.36	91.32
LS21	53.61	0.17	2.99	1.28	1.99	0.07	15.49	20.89	1.65	0.00	0.04	98.18	93.28
LS22	51.17	0.72	6.15	0.61	2.62	0.09	14.90	21.09	1.39	0.00	0.04	98.80	91.03
LS23	53.01	0.63	7.05	0.73	2.79	0.03	14.92	20.32	1.71	0.01	0.04	101.24	90.50
LS24	51.69	0.63	6.79	0.50	2.77	0.09	14.81	20.41	1.65	0.00	0.04	99.39	90.50
LS26	53.31	0.01	2.11	0.63	2.10	0.09	17.61	23.85	0.16	0.00	0.04	99.90	93.72
LS30	51.89	0.44	6.30	0.66	2.71	0.08	14.65	20.22	1.63	0.00	0.03	98.61	90.59
LS31	51.93	0.53	6.86	0.59	2.44	0.08	13.99	20.58	1.96	0.01	0.03	99.00	91.08
FS01	52.80	0.40	6.47	0.97	2.53	0.09	14.95	19.70	1.92	0.01	0.03	99.86	91.32
FS03	51.61	0.15	6.54	1.18	3.22	0.12	17.16	18.57	0.80	0.01	0.04	99.40	90.48
FS06	53.67	0.03	4.18	1.38	2.54	0.07	16.35	20.53	0.99	0.01	0.03	99.78	92.00
FS07	52.78	0.47	6.67	0.81	2.77	0.07	14.82	19.84	1.29	0.01	0.03	99.56	90.51
FS11	52.42	0.47	6.00	1.05	2.76	0.09	16.03	20.40	1.62	0.01	0.05	100.90	91.18
FS12	51.94	0.34	7.22	0.91	3.11	0.10	16.39	18.37	1.11	0.02	0.04	99.55	90.39
FS13	52.22	0.42	7.43	0.75	3.22	0.10	15.59	18.74	1.39	0.01	0.05	99.91	89.63
FS14	51.85	0.51	6.89	0.94	3.32	0.08	15.39	18.93	1.33	0.00	0.01	99.26	89.20
FS16	52.95	0.24	4.94	1.28	2.64	0.09	15.96	20.16	1.14	0.01	0.04	99.45	91.50
FS17	52.65	0.43	6.55	1.07	2.50	0.08	14.92	20.14	1.49	0.00	0.03	99.87	91.40
FS18	51.38	0.52	7.94	0.86	3.67	0.10	16.76	17.63	1.63	0.02	0.07	100.57	89.06
FS19	51.89	0.49	7.42	0.80	3.58	0.10	15.66	18.67	1.14	0.01	0.03	99.79	88.64
FS21	52.23	0.51	6.93	0.80	2.92	0.09	15.03	19.32	1.63	0.00	0.02	99.49	90.16
FS23	52.62	0.20	5.39	1.60	3.20	0.12	16.29	18.75	1.30	0.00	0.02	99.49	90.09
FS24	53.68	0.03	2.50	0.60	2.11	0.07	17.75	24.12	0.26	0.01	0.05	101.17	93.76
FS26	52.09	0.56	6.88	0.74	2.65	0.09	14.82	20.17	1.50	0.01	0.02	99.52	90.89
Penglai													
PL01	52.13	0.47	6.84	0.49	2.72	0.08	14.83	20.54	1.84	0.00	0.03	99.98	90.67
PL10	52.20	0.44	6.28	0.44	2.58	0.11	15.36	20.90	1.55	0.01	0.03	99.88	91.39
PL17	52.39	0.47	6.66	0.44	2.66	0.08	14.91	20.64	1.80	0.00	0.03	100.09	90.90
PL19	52.00	0.52	6.95	0.58	2.62	0.10	14.71	20.58	1.86	0.01	0.02	99.94	90.92
PL32	52.19	0.47	5.66	0.55	2.81	0.08	15.38	20.94	1.50	0.01	0.03	99.61	90.71
PL36	52.14	0.47	6.86	0.48	2.65	0.09	14.80	20.30	1.81	0.01	0.03	99.65	90.89
PL42	52.00	0.46	6.38	0.42	2.48	0.07	15.39	20.78	1.44	0.00	0.03	99.47	91.71
PL44	52.05	0.62	7.51	0.42	2.75	0.08	14.60	20.13	1.99	0.00	0.03	100.18	90.44
PL46	53.48	0.05	3.30	0.76	2.26	0.08	16.66	22.09	1.14	0.01	0.03	99.87	92.94
Changle													
CL01	53.58	0.18	4.99	0.63	2.74	0.10	15.87	21.08	0.89	0.00	0.03	100.08	91.16
CL22	52.09	0.61	6.40	0.48	2.45	0.08	14.78	19.97	1.15	0.00	0.02	98.00	91.50
CL31	53.21	0.29	5.72	0.44	2.58	0.08	15.28	19.63	2.00	0.00	0.00	99.23	91.35
CL32	52.39	0.49	6.34	0.40	2.39	0.08	14.45	21.40	1.25	0.01	0.05	99.26	91.51
CL35	53.26	0.31	6.50	0.44	2.34	0.11	14.40	19.12	2.68	0.00	0.00	99.17	91.64
CL38	52.45	0.42	5.92	0.57	2.30	0.06	14.34	21.20	1.16	0.00	0.02	98.43	91.76

Table 2. (continued)

Sample	SiO_2	TiO_2	Al_2O_3	Cr_2O_3	FeO	MnO	MgO	CaO	Na_2O	K_2O	NiO	TOTAL	Mg #
							Qixia						
QX01	53.18	0.04	2.72	0.47	2.18	0.07	17.33	23.59	0.12	0.01	0.00	99.72	93.41
QX04	54.51	0.14	4.04	0.57	2.12	0.11	15.62	22.32	0.72	0.00	0.01	100.15	92.94
QX14	52.40	0.49	6.72	0.40	2.30	0.10	14.21	21.23	1.41	0.00	0.02	99.27	91.68
QX18	53.10	0.05	2.65	0.47	2.20	0.10	16.94	23.44	0.23	0.00	0.04	99.23	93.23
QX49	52.76	0.41	5.14	0.57	2.27	0.08	15.13	22.60	0.93	0.00	0.01	99.89	92.25
QX50	53.75	0.03	2.11	0.73	2.03	0.08	16.90	23.52	0.19	0.01	0.06	99.41	93.69
QX51	52.02	0.48	5.43	0.50	2.47	0.06	14.99	22.28	0.95	0.00	0.00	99.18	91.53
QX60	53.04	0.08	4.29	0.00	3.12	0.08	14.70	23.60	0.78	0.00	0.00	99.70	89.37
							Hebi						
HB01	53.71	0.03	3.32	1.41	2.08	0.05	16.78	21.00	0.66	0.00	0.04	99.11	93.50
HB02	55.25	0.02	1.81	0.36	1.97	0.05	17.06	22.39	0.37	0.00	0.04	99.34	93.92
HB17	53.64	0.12	4.19	0.84	2.42	0.10	16.46	20.29	0.95	0.00	0.05	99.06	92.39
HB64	47.24	5.26	5.53	0.73	2.87	0.05	13.81	23.22	0.65	0.01	0.03	99.40	89.57

[a]Mg # = 100Mg/(Mg + Fe). Panshishan and Lianshan samples are also included because only Al_2O_3 and MgO contents of clinopyroxenes of have been given by *Bonadiman et al.* [2009].

25–94 ppm; Hebei, 31–96 ppm). *Aubaud et al.* [2007], *Yang et al.* [2008] and *Bonadiman et al.* [2009] reported similar values for the NCC peridotites. The cpx and opx water contents are strongly correlated (R^2 = 0.89) with a cpx/opx ratio of 2.29 (Figure 4a). Taking into account all the values measured on peridotites from the NCC [*Aubaud et al.*, 2007; *Yang et al.*, 2008; *Bonadiman et al.*, 2009; this study], this ratio is 1.97 (R^2 = 0.77, Figure 4b). These ratios agree well with the H partition coefficient between cpx and opx reported from both experimental and natural mantle samples [*Bell and Rossman*, 1992a; *Peslier et al.*, 2002; *Koga et al.*, 2003; *Aubaud et al.*, 2004, 2007; *Bell et al.*, 2004; *Grant et al.*, 2007b; *Tenner et al.*, 2009]. The water distribution in pyroxenes from the NCC peridotites thus achieved equilibrium in the mantle and was preserved during xenolith exhumation. The latter is confirmed by the homogeneous distribution of water within individual pyroxene grains revealed by core-rim profile analyses [*Yang et al.*, 2008; *Bonadiman et al.*, 2009; this study].

[22] In agreement with previous results from samples from Nushan, Hannuoba, Panshishan, and Lianshan from the NCC [*Aubaud et al.*, 2007; *Yang et al.*, 2008; *Bonadiman et al.*, 2009], ol grains in this study display very low water contents: only a few grains from Fangshan and Changle peridotites display weak OH absorption bands and the H_2O contents are less than 2 ppm (Figure 3c). Because we used the average value of more than 25 ol grains for each peridotite to represent the water content of ol in that sample, H_2O contents of ol in all samples are ~0 ppm even for those containing ol grains with ~2 ppm H_2O. The water content of ol from spinel peridotite xenoliths hosted by alkaline basalts is typically lower than 10 ppm [*Bell and Rossman*, 1992a; *Peslier and Luhr*, 2006; *Grant et al.*, 2007b; *Gose et al.*, 2009a], due to possible initial low water contents or to possible H loss by diffusion during xenolith ascent to the surface [e.g., *Demouchy et al.*, 2006; *Peslier and Luhr*, 2006]. In contrast, pyroxenes coexisting with olivine appear to retain their initial H contents to a much larger extent [*Peslier et al.*, 2002; *Bell et al.*, 2004; *Grant et al.*, 2007b; *Yang et al.*, 2008; *Bonadiman et al.*, 2009; *Gose et al.*, 2009b]. In our case, the OH contents measured in ol (~0 ppm) cannot represent their source value. Instead, an initial H_2O content can be calculated for ol by considering equilibrium partitioning between pyroxenes and ol.

[23] The H_2O partition coefficients between pyroxene and olivine determined by experiments are highly variable. The values obtained at low pressure (<3 GPa) are much higher than those at high pressure (>8GPa): At low pressures, *Koga et al.* [2003] obtained a value of 12 ± 2 for Dopx/ol from a single experiment at P = 1.8 GPa; *Aubaud et al.* [2004] (revised according to the new calibration of *Aubaud et al.* [2007]) determined Dcpx/ol and Dopx/ol of 28 ± 2 (n = 2) and 14 ± 2 (n = 4), respectively, at P = 1–1.5 GPa; *Hauri et al.* [2006] reported Dcpx/ol and Dopx/ol of 15 ± 5 (n = 5) and 10 ± 3 (n = 8) respectively at P = 0.5–1.6 GPa; *Grant et al.* [2007a] determined Dopx/ol = 25 ± 1 (n = 2) at P = 1.5 GPa; *Tenner et al.* [2009] obtained Dcpx/ol of 27 (n = 1) at P = 3 GPa. In contrast, at higher pressures, *Withers and Hirschmann* [2007] reported Dopx/ol of 1.3 ± 0.2 (n = 4) at P = 8.0–12 GPa; and *Withers and Hirschmann* [2008] obtained Dopx/ol of 1.5 ± 0.2 (n = 3) at P = 8.0 GPa. The difference between low-pressure and high-pressure experiments is probably related to reduced pyroxene Al content at P > 3 GPa (see data summarized in Figure 7 of *Hirschmann et al.* [2009]): it has been confirmed by experiments that Al could enhance water solubility in pyroxene (see data summarized in Figure 2 of *Hirschmann et al.* [2009]). *Grant et al.* [2007b] have shown that ol, opx and cpx from 8 peridotite xenoliths preserved the H_2O contents of their mantle source and had Dcpx/ol values of 88 ± 48 and 22 ± 24 for spinel peridotites (P = 1.1–2.8 GPa) and garnet peridotites (P = 3.7–7.4 GPa), respectively.

[24] The NCC spinel lherzolite xenoliths hosted by Cenozoic basalts are from relatively thin lithospheric mantle (<80–100 km [*Menzies et al.*, 2007]), and the partition coefficient of H_2O between pyroxene and olivine should be similar to those determined by low-pressure experiments (i.e., Dcpx/ol > 10 [*Koga et al.*, 2003; *Hauri et al.* 2006; *Aubaud et al.*, 2007; *Grant et al.*, 2007a; *Tenner et al.* 2009]). In the following, we use a Dcpx/ol = 10 to calculate the H_2O content of coexisting ol; the calculated values should therefore represent maximum estimates. The recalculated whole-rock H_2O contents based on mineral modes should also represent maximum estimates. These recalculated

Table 3. Major Element Concentrations of Orthopyroxenes From Peridotite Xenoliths Hosted by Cenozoic Basalts of the Eastern NCC[a]

Sample	SiO_2	TiO_2	Al_2O_3	Cr_2O_3	FeO	MnO	MgO	CaO	Na_2O	K_2O	NiO	TOTAL	Mg #
							Panshishan						
PSS01	56.10	0.11	4.29	0.39	6.22	0.15	33.27	0.61	0.08	0.00	0.08	101.31	90.51
PSS02	56.54	0.08	4.21	0.37	6.22	0.16	33.44	0.61	0.07	0.00	0.08	101.80	90.55
PSS05	55.65	0.07	4.46	0.35	5.91	0.15	32.61	0.62	0.08	0.01	0.08	99.99	89.98
PSS07	55.54	0.12	4.31	0.35	5.96	0.14	32.31	0.64	0.10	0.01	0.07	99.55	90.62
PSS10	56.09	0.12	4.31	0.30	6.02	0.14	31.99	0.63	0.11	0.01	0.09	99.80	90.45
PSS11	55.34	0.10	3.66	0.31	6.19	0.16	34.30	0.43	0.05	0.00	0.11	100.66	90.81
PSS12	54.96	0.12	4.60	0.35	6.07	0.17	32.53	0.60	0.06	0.01	0.05	99.51	89.98
PSS13	56.94	0.12	4.33	0.30	6.07	0.14	31.62	0.63	0.11	0.01	0.07	100.34	90.28
PSS15	55.66	0.15	3.88	0.33	6.33	0.14	34.10	0.46	0.05	0.00	0.09	101.19	90.57
PSS16	57.72	0.12	4.26	0.29	6.18	0.14	31.31	0.62	0.10	0.00	0.07	100.82	90.04
PSS17	56.84	0.06	3.37	0.45	5.74	0.08	33.99	0.60	0.03	0.00	0.06	101.23	91.34
PSS18	55.58	0.10	3.65	0.21	6.52	0.17	33.07	0.37	0.00	0.00	0.06	99.73	89.98
PSS19	57.71	0.10	4.26	0.34	6.20	0.14	31.22	0.61	0.11	0.01	0.07	100.77	89.98
PSS20	55.79	0.16	3.58	0.39	6.33	0.14	34.31	0.46	0.03	0.00	0.09	101.28	90.63
							Lianshan						
LS01	54.73	0.08	3.96	0.38	6.29	0.12	32.66	0.51	0.08	0.01	0.05	98.87	90.24
LS02	55.34	0.09	4.09	0.31	6.40	0.16	32.86	0.47	0.08	0.00	0.06	99.87	90.15
LS03	57.27	0.05	2.89	0.49	5.35	0.12	34.48	0.59	0.05	0.01	0.14	101.43	92.00
LS04	54.93	0.13	4.50	0.30	6.34	0.15	32.62	0.65	0.11	0.00	0.08	99.81	90.18
LS05	55.23	0.08	3.79	0.26	6.38	0.16	34.01	0.47	0.06	0.02	0.07	100.54	90.48
LS06	55.01	0.11	4.29	0.41	5.95	0.13	32.74	0.64	0.10	0.01	0.07	99.47	90.75
LS07	55.08	0.11	4.30	0.32	6.19	0.15	32.99	0.63	0.10	0.00	0.08	99.95	90.48
LS08	55.46	0.10	4.02	0.23	6.11	0.15	33.28	0.53	0.08	0.01	0.07	100.04	90.66
LS12	56.09	0.03	3.37	0.51	5.57	0.13	34.78	0.60	0.04	0.00	0.10	101.20	91.76
LS17	56.13	0.03	2.72	0.54	5.44	0.15	35.33	0.65	0.04	0.00	0.06	101.10	92.05
LS19	53.70	0.05	2.56	0.42	6.40	0.13	36.00	0.46	0.05	0.00	0.10	99.87	90.93
LS20	56.74	0.05	3.59	0.51	5.99	0.11	33.89	0.64	0.13	0.01	0.12	101.78	90.99
LS21	56.29	0.04	1.88	0.24	5.34	0.13	34.09	0.48	0.07	0.01	0.07	98.64	91.93
LS22	54.61	0.15	4.10	0.22	6.60	0.16	32.47	0.55	0.07	0.01	0.06	98.99	89.77
LS23	56.17	0.13	4.49	0.31	6.45	0.16	33.37	0.59	0.06	0.01	0.05	101.79	90.22
LS24	54.97	0.10	4.39	0.26	6.32	0.15	33.00	0.58	0.09	0.00	0.08	99.94	90.30
LS26	56.01	0.00	2.29	0.47	5.63	0.14	34.33	0.57	0.01	0.00	0.08	99.54	91.58
LS30	54.75	0.09	4.38	0.30	6.07	0.13	31.74	0.66	0.10	0.01	0.09	98.31	90.32
LS31	55.42	0.13	3.72	0.21	6.69	0.15	32.79	0.44	0.07	0.00	0.06	99.68	89.73
							Fangshan						
FS01	55.54	0.09	4.35	0.45	5.71	0.15	32.73	0.64	0.14	0.00	0.03	99.82	91.43
FS03	54.33	0.07	5.78	0.75	5.36	0.14	31.72	1.48	0.08	0.00	0.08	99.79	91.43
FS06	55.93	0.00	3.11	0.67	5.40	0.13	33.19	0.87	0.08	0.00	0.07	99.46	91.43
FS07	54.41	0.13	4.81	0.38	6.25	0.15	32.18	0.72	0.08	0.00	0.07	99.20	91.43
FS11	55.40	0.13	4.20	0.51	6.02	0.12	33.96	0.73	0.11	0.00	0.11	101.29	90.95
FS12	54.40	0.11	5.80	0.56	5.80	0.14	31.35	1.24	0.13	0.00	0.08	99.61	91.43
FS13	54.57	0.11	5.78	0.43	5.95	0.16	31.63	1.05	0.16	0.00	0.07	99.90	91.43
FS14	54.64	0.14	5.06	0.54	6.08	0.17	31.82	0.93	0.12	0.00	0.08	99.57	91.43
FS16	55.62	0.10	3.61	0.63	5.02	0.16	33.11	0.80	0.10	0.01	0.07	99.23	91.43
FS17	55.23	0.10	4.36	0.41	5.74	0.13	32.51	0.64	0.10	0.00	0.06	99.29	91.43
FS18	53.82	0.22	6.33	0.53	6.39	0.15	31.92	1.39	0.19	0.01	0.12	101.08	89.90
FS19	53.78	0.16	5.90	0.44	5.90	0.14	31.57	1.12	0.09	0.00	0.08	99.18	91.43
FS21	54.72	0.13	4.86	0.37	6.09	0.15	32.24	0.78	0.13	0.01	0.06	99.52	91.43
FS23	55.72	0.10	3.81	0.82	5.69	0.14	32.65	1.06	0.13	0.01	0.05	100.18	91.43
FS24	56.34	0.01	2.84	0.40	5.84	0.13	34.94	0.53	0.01	0.00	0.11	101.16	91.43
FS26	54.93	0.13	4.61	0.30	6.06	0.15	32.45	0.62	0.10	0.00	0.07	99.43	91.43
							Penglai						
PL01	55.25	0.08	4.29	0.20	6.40	0.16	33.23	0.51	0.08	0.01	0.04	100.24	90.26
PL10	55.53	0.11	4.34	0.20	5.86	0.14	33.22	0.54	0.08	0.00	0.05	100.06	91.00
PL17	55.82	0.11	4.16	0.17	6.24	0.14	32.90	0.46	0.07	0.01	0.07	100.16	90.38
PL19	55.69	0.09	4.04	0.21	6.21	0.13	33.19	0.50	0.07	0.00	0.07	100.21	90.51
PL32	55.63	0.11	3.75	0.25	6.61	0.16	33.25	0.57	0.06	0.01	0.05	100.45	89.97
PL36	55.28	0.07	4.18	0.13	6.35	0.12	33.17	0.46	0.07	0.00	0.05	99.89	90.30
PL42	54.94	0.11	4.61	0.19	6.01	0.17	33.30	0.56	0.07	0.00	0.09	100.04	90.80
PL44	55.35	0.11	4.46	0.14	6.37	0.15	33.22	0.49	0.08	0.00	0.06	100.43	90.28
PL46	56.42	0.03	2.36	0.33	5.46	0.15	34.25	0.59	0.03	0.01	0.07	99.69	91.80
							Changle						
CL01	55.53	0.06	3.97	0.23	5.74	0.15	32.82	0.62	0.10	0.01	0.06	99.29	91.06
CL22	54.94	0.12	4.29	0.24	6.74	0.15	31.52	0.75	0.08	0.01	0.06	98.89	89.29
CL31	55.42	0.05	3.92	0.25	6.19	0.15	32.49	0.70	0.09	0.01	0.06	99.34	90.34
CL32	56.08	0.07	3.82	0.17	6.23	0.16	32.75	0.54	0.04	0.00	0.07	99.90	90.37
CL35	56.00	0.02	3.92	0.20	5.79	0.15	32.80	0.57	0.13	0.00	0.01	99.57	90.99
CL38	55.60	0.09	3.55	0.21	6.41	0.19	33.17	0.47	0.02	0.01	0.04	99.74	90.22

Table 3. (continued)

Sample	SiO_2	TiO_2	Al_2O_3	Cr_2O_3	FeO	MnO	MgO	CaO	Na_2O	K_2O	NiO	TOTAL	Mg #
							Qixia						
QX01	56.91	0.03	2.44	0.27	5.61	0.13	34.08	0.59	0.02	0.01	0.07	100.15	91.55
QX04	56.34	0.05	3.01	0.21	5.66	0.11	33.54	0.50	0.01	0.00	0.03	99.45	91.35
QX14	55.83	0.10	3.87	0.16	6.25	0.17	33.24	0.52	0.05	0.01	0.07	100.24	90.47
QX18	56.63	0.01	2.52	0.22	5.69	0.14	33.50	0.57	0.01	0.01	0.06	99.35	91.30
QX49	55.84	0.08	3.65	0.25	6.13	0.18	33.04	0.43	0.03	0.01	0.01	99.65	90.58
QX50	56.70	0.03	2.16	0.27	5.72	0.15	34.17	0.60	0.00	0.00	0.04	99.83	91.42
QX51	55.62	0.09	3.70	0.17	6.23	0.13	33.19	0.42	0.01	0.01	0.05	99.62	90.47
							Hebi						
HB01	56.52	0.01	2.18	0.52	5.09	0.12	33.30	0.92	0.05	0.00	0.07	98.81	92.10
HB02	58.44	0.00	0.88	0.23	4.82	0.12	34.48	0.52	0.02	0.00	0.07	99.56	92.73
HB06	56.15	0.02	3.27	0.79	4.53	0.09	33.41	0.91	0.05	0.01	0.06	99.32	92.93
HB07	56.05	0.06	3.19	0.14	5.26	0.08	34.25	0.26	0.00	0.01	0.07	99.37	92.07
HB10	58.61	0.00	0.66	0.25	4.53	0.12	35.41	0.21	0.00	0.00	0.06	99.86	93.31
HB17	56.36	0.05	3.31	0.45	4.70	0.11	33.48	0.92	0.08	0.01	0.07	99.54	92.70
HB64	55.28	0.06	3.77	0.67	7.01	0.17	31.17	0.86	0.19	0.01	0.04	99.22	88.80

[a]Mg # = 100Mg/(Mg + Fe). Panshishan and Lianshan samples are also included because only Al_2O_3 and MgO contents of orthopyroxenes have been given by *Bonadiman et al.* [2009].

whole-rock H_2O contents for the NCC peridotite xenoliths range between 6 and 85 ppm with an average value of 25 ± 18 ppm (Table 5).

5. Discussion

5.1. Preservation of Initial Water Content of the Mantle Source

[25] For P < 3.5 GPa, the solubility of hydrogen in nominally anhydrous minerals (NAMs) increases with increasing pressure [*Keppler and Bolfan-Casanova*, 2006, and references therein; *Mierdel et al.*, 2007]; thus, when peridotite xenoliths are transported to the surface by their host magmas, hydrogen can potentially diffuse out the NAMs due to the sharp pressure fall. Diffusion experiments predict that at 1000°C hydrogen resetting in olivine and pyroxene will be achieved at millimeter scale in a few tens of hours [*Kohlstedt and Mackwell*, 1998; *Hercule and Ingrin*, 1999; *Carpenter et al.*, 2000; *Stalder and Skogby*, 2003]. In contrast, studies on natural samples suggest that pyroxenes preserve their mantle-derived OH contents, but ol do not [*Bell and Rossman*, 1992a; *Bell et al.*, 2004; *Peslier et al.*, 2002; *Grant et al.*, 2007b; *Gose et al.*, 2009b]. Possible explanations for the discrepancy may be related to the facts that (1) the loss of hydrogen is influenced by the water and oxygen fugacities of the systems and the H content of coexisting minerals and melt; (2) the incorporation of hydrogen into minerals does not only depend on the diffusion rate of hydrogen, but also on the diffusion rate of point defects associated with hydrogen incorporation, the latter being comparatively slower by at least several orders of magnitude [*Kohlstedt and Mackwell*, 1998]; and (3) experiments are made under H_2O-saturated conditions, which probably do not prevail in natural systems.

[26] On the other hand, several lines of evidence suggest that pyroxenes of the NCC peridotites have largely preserved their initial water content in the mantle source.

[27] 1. H_2O contents are homogeneous within individual pyroxene grains. Core-rim profile analysis for cpx and opx grains of the NCC peridotites [*Yang et al.*, 2008; *Bonadiman et al.*, 2009; this study] have not revealed significant heterogeneities in H_2O distribution within single grains, the latter normally being ascribed to diffusion.

[28] 2. H_2O contents are positively correlated between cpx and opx. As shown in Figure 4, H_2O contents of cpx and opx display a good positive correlation. The partition coefficient between cpx and opx (Dcpx/opx) is 2.29 in considering only the data from this study, and 1.97 considering all the NCC data together. This is in the same range as the literature values reported for natural peridotite xenoliths: Dcpx/opx = 2.3 ± 0.5 (n = 38 [*Bell and Rossman*, 1992a; *Peslier et al.*, 2002; *Grant et al.*, 2007b; *Li et al.*, 2008]), and also close to those determined by experiments using a low-blank SIMS method: *Aubaud et al.* [2004] reported Dcpx/opx = 1.8 ± 0.3 [n = 1, the value is revised according to new calibration of *Aubaud et al.* 2007]; *Hauri et al.* [2006] obtained Dcpx/opx = 0.9–1.4 (n = 6); *Tenner et al.* [2009] reported Dcpx/opx = 1.2–2.0 (n = 3).

[29] On the basis of heterogeneous distribution of H_2O within single grains (higher contents in the core and lower contents in the rim), several studies suggested significant loss of hydrogen in olivines by diffusion during xenolith ascent to the surface [*Demouchy et al.*, 2006; *Peslier and Luhr*, 2006; *Peslier et al.*, 2008]. Other studies did not observe any water heterogeneity in their olivines [*Bell et al.*, 2004; *Grant et al.*, 2007b]. We cannot address this issue based on the NCC olivines because their water contents are too low to be detected.

5.2. Comparison With Continental Lithospheric Mantle and Oceanic Mantle

[30] *Yang et al.* [2008] noticed that the Nushan and Hannuoba peridotites have much lower water contents than peridotites from cratonic and off-cratonic continental areas worldwide. Combining the previously published data [*Aubaud et al.*, 2007; *Yang et al.*, 2008; *Bonadiman et al.*, 2009] with our data, we obtain a total of 105 peridotites hosted by Cenozoic basalts from 9 localities of the eastern part of the NCC, which we use to make the following observations and interpretations. As described below, the

Table 4. Major Element Concentrations of Spinels From Peridotite Xenoliths Hosted by Cenozoic Basalts of the Eastern NCC[a]

Sample	SiO_2	TiO_2	Al_2O_3	Cr_2O_3	FeO	MnO	MgO	CaO	Na_2O	K_2O	NiO	Total	Cr #
Panshishan													
PSS01	0.29	0.16	56.44	11.48	10.14	0.08	20.10	0.01	0.01	0.00	0.36	99.09	12.01
PSS02	0.28	0.11	56.05	12.07	10.79	0.15	19.78	0.02	0.00	0.01	0.28	99.53	12.62
PSS05	0.06	0.08	59.27	10.50	9.80	0.12	20.57	0.00	0.02	0.01	0.22	100.63	10.62
PSS07	0.05	0.07	54.46	13.15	11.34	0.12	19.08	0.00	0.01	0.00	0.31	98.60	13.94
PSS10	0.06	0.21	48.18	20.79	11.15	0.11	18.41	0.00	0.01	0.01	0.23	99.15	22.45
PSS11	0.02	0.09	56.52	10.57	10.61	0.06	21.85	0.01	0.00	0.00	0.38	100.11	11.15
PSS12	0.03	0.14	58.59	9.90	10.77	0.12	20.34	0.00	0.00	0.01	0.25	100.15	10.18
PSS13	0.05	0.07	53.37	15.16	10.46	0.11	19.18	0.00	0.00	0.00	0.28	98.69	16.01
PSS15	0.00	0.08	57.08	10.72	10.64	0.07	21.52	0.01	0.00	0.00	0.40	100.51	11.19
PSS16	0.07	0.17	57.44	9.11	11.09	0.11	19.61	0.00	0.01	0.00	0.31	97.93	9.62
PSS17	0.25	0.10	46.96	21.85	11.60	0.12	18.83	0.02	0.02	0.01	0.26	100.00	23.78
PSS18	0.01	0.08	55.17	14.30	11.33	0.16	19.28	0.00	0.00	0.01	0.17	100.51	14.81
PSS19	0.02	0.03	60.36	7.77	9.71	0.10	20.10	0.01	0.01	0.00	0.36	98.47	7.95
Lianshan													
LS01	0.05	0.09	53.43	14.38	11.46	0.13	18.90	0.00	0.01	0.00	0.30	98.76	15.29
LS02	0.08	0.05	58.15	10.12	10.14	0.12	19.83	0.00	0.02	0.01	0.31	98.82	10.45
LS03	0.27	0.13	39.33	28.33	13.20	0.21	17.98	0.01	0.00	0.01	0.23	99.69	32.57
LS04	0.07	0.14	58.01	9.42	11.14	0.09	20.94	0.00	0.00	0.00	0.32	100.14	9.83
LS05	0.05	0.07	57.67	9.57	10.72	0.06	21.11	0.01	0.00	0.00	0.37	99.61	10.01
LS06	0.06	0.11	55.03	12.47	10.53	0.12	19.48	0.00	0.01	0.00	0.31	98.13	13.20
LS07	0.09	0.12	55.78	12.37	10.72	0.12	20.69	0.00	0.01	0.00	0.29	100.19	12.95
LS08	0.03	0.06	53.83	14.18	11.23	0.11	19.28	0.00	0.01	0.01	0.29	99.04	15.02
LS12	0.02	0.06	45.71	21.93	12.21	0.02	19.75	0.00	0.00	0.00	0.34	100.04	24.35
LS17	0.01	0.03	37.07	31.91	12.19	0.00	18.44	0.01	0.00	0.00	0.22	99.89	36.60
LS19	0.04	0.09	44.09	25.72	12.42	0.17	17.69	0.00	0.02	0.01	0.19	100.44	28.12
LS20	0.22	0.10	47.24	20.81	12.11	0.11	18.68	0.00	0.00	0.01	0.25	99.53	22.81
LS21	0.04	0.14	29.55	41.24	13.97	0.23	15.19	0.00	0.01	0.00	0.09	100.47	48.35
LS22	0.07	0.27	54.29	12.94	11.21	0.12	18.92	0.03	0.00	0.01	0.25	98.09	13.78
LS23	0.06	0.13	59.68	8.40	10.56	0.15	20.47	0.00	0.01	0.01	0.39	99.87	8.63
LS24	0.05	0.11	58.55	8.72	10.35	0.12	20.01	0.00	0.01	0.01	0.31	98.25	9.08
LS26	0.03	0.04	34.48	35.29	14.66	0.20	15.96	0.00	0.02	0.00	0.16	100.83	40.71
LS30	0.08	0.11	55.81	11.69	10.66	0.11	19.68	0.00	0.01	0.00	0.32	98.48	12.32
LS31	0.03	0.06	57.89	8.93	11.23	0.12	19.27	0.00	0.00	0.00	0.33	97.88	9.38
Fangshan													
FS01	0.05	0.14	54.64	14.75	10.87	0.14	20.20	0.01	0.00	0.00	0.22	101.02	15.33
FS03	0.16	0.13	50.42	18.30	10.86	0.13	20.47	0.00	0.01	0.00	0.24	100.72	19.58
FS06	0.04	0.03	36.61	32.58	13.66	0.22	17.24	0.00	0.00	0.01	0.14	100.54	37.38
FS07	0.08	0.13	56.51	11.44	10.30	0.12	20.72	0.00	0.01	0.00	0.24	99.54	11.95
FS11	0.04	0.20	50.70	16.69	11.39	0.05	20.70	0.01	0.00	0.00	0.36	100.15	18.09
FS12	0.12	0.15	56.84	12.27	10.06	0.12	20.85	0.00	0.01	0.00	0.23	100.66	12.65
FS13	0.08	0.19	58.66	9.65	10.66	0.07	20.99	0.00	0.01	0.01	0.25	100.56	9.93
FS14	0.08	0.25	54.25	14.04	11.37	0.15	20.13	0.00	0.02	0.01	0.22	100.53	14.79
FS16	0.06	0.17	43.12	26.20	11.64	0.14	18.84	0.00	0.00	0.01	0.17	100.35	28.96
FS17	0.05	0.12	54.63	14.34	10.53	0.13	19.99	0.01	0.00	0.01	0.22	100.03	14.98
FS18	0.12	0.26	56.99	9.89	10.87	0.06	21.74	0.00	0.00	0.00	0.36	100.27	10.42
FS19	0.11	0.18	57.23	10.01	10.75	0.12	20.85	0.02	0.00	0.00	0.24	99.51	10.50
FS21	0.05	0.15	57.30	10.42	10.96	0.13	20.50	0.00	0.01	0.00	0.25	99.78	10.87
FS23	0.09	0.24	38.47	29.64	14.23	0.17	17.90	0.00	0.01	0.00	0.17	100.90	34.08
FS24	0.01	0.01	44.06	24.15	12.16	0.03	19.06	0.00	0.00	0.00	0.25	99.75	26.89
FS26	0.04	0.14	59.40	9.41	10.21	0.10	20.68	0.00	0.00	0.00	0.24	100.22	9.60
Penglai													
PL01	0.02	0.07	61.42	5.34	11.58	0.12	20.89	0.00	0.00	0.00	0.27	99.71	5.51
PL10	0.03	0.09	59.80	6.12	12.17	0.11	20.64	0.00	0.01	0.00	0.27	99.24	6.42
PL17	0.03	0.06	61.43	5.41	12.77	0.12	20.45	0.00	0.01	0.00	0.28	100.56	5.58
PL19	0.02	0.08	60.25	6.46	12.85	0.12	20.53	0.01	0.00	0.00	0.28	100.58	6.71
PL32	0.06	0.83	50.02	16.16	13.92	0.16	18.85	0.04	0.00	0.01	0.22	100.27	17.81
PL36	0.01	0.07	58.81	2.95	11.91	0.10	19.89	0.00	0.00	0.00	0.15	93.89	3.26
PL42	0.03	0.10	62.07	5.68	11.47	0.10	20.85	0.00	0.01	0.01	0.28	100.59	5.79
PL44	0.03	0.07	63.53	4.61	10.54	0.11	20.90	0.01	0.02	0.01	0.29	100.12	4.64
PL46	0.01	0.09	32.96	35.78	14.32	0.22	16.64	0.00	0.01	0.00	0.14	100.16	42.14
Changle													
CL01	0.05	0.05	52.89	15.79	10.54	0.20	19.31	0.02	0.00	0.02	0.18	99.05	16.68
CL22	0.03	0.13	54.90	13.39	12.74	0.14	19.24	0.00	0.00	0.01	0.25	100.82	14.06
CL31	0.03	0.10	52.55	16.13	11.26	0.15	19.58	0.00	0.01	0.00	0.19	100.02	17.08
CL35	0.01	0.02	46.51	23.81	10.29	0.17	19.09	0.00	0.01	0.01	0.15	100.07	25.56
CL38	0.02	0.05	54.77	14.55	10.57	0.15	19.58	0.00	0.01	0.00	0.21	99.92	15.12

Table 4. (continued)

Sample	SiO_2	TiO_2	Al_2O_3	Cr_2O_3	FeO	MnO	MgO	CaO	Na_2O	K_2O	NiO	Total	Cr #
							Qixia						
QX01	0.04	0.06	35.83	34.63	13.67	0.20	16.53	0.00	0.01	0.01	0.12	101.10	39.33
QX04	0.00	0.05	47.59	22.56	11.97	0.20	18.12	0.00	0.00	0.00	0.16	100.65	24.13
QX18	0.00	0.07	37.96	31.22	14.38	0.18	16.84	0.00	0.03	0.02	0.15	100.85	35.55
QX50	0.02	0.10	33.41	36.54	15.07	0.25	15.94	0.00	0.03	0.00	0.12	101.47	42.32
							Hebi						
HB01	0.04	0.06	28.47	41.44	13.58	0.20	16.45	0.01	0.03	0.01	0.15	100.49	49.41
HB02	0.02	0.06	24.31	44.52	14.55	0.23	15.74	0.00	0.00	0.01	0.10	99.61	55.12
HB06	0.03	0.15	33.77	35.49	12.05	0.24	17.95	0.00	0.00	0.01	0.15	99.89	41.35
HB07	0.03	0.14	51.40	16.60	11.72	0.09	19.70	0.00	0.00	0.00	0.19	99.87	17.80
HB10	0.03	0.00	18.71	49.65	15.65	0.27	14.96	0.02	0.00	0.01	0.12	99.47	64.03
HB12	0.04	0.03	32.09	37.37	12.70	0.23	17.49	0.01	0.00	0.00	0.13	100.09	43.86
HB16	0.04	0.01	25.91	44.76	13.08	0.25	16.23	0.00	0.00	0.00	0.12	100.39	53.68
HB17	0.04	0.19	34.47	35.89	12.07	0.21	17.95	0.01	0.01	0.00	0.18	101.03	41.12
HB64	0.05	0.83	35.94	29.10	18.33	0.23	15.87	0.00	0.01	0.00	0.13	100.48	35.20

[a]Cr # = 100 Cr/(Cr + Al). Panshishan and Lianshan samples are also included because no spinel data have been given by *Bonadiman et al.* [2009].

Cenozoic lithospheric mantle of the NCC (at least the eastern part) appears to have lower water contents compared to both the continental cratonic and off-cratonic lithospheric mantle worldwide and to the oceanic mantle.

5.2.1. Comparison With the Continental Cratonic and Off-Cratonic Lithospheric Mantle

[31] Water contents of peridotites from the NCC [*Aubaud et al.*, 2007; *Yang et al.*, 2008; *Bonadiman et al.*, 2009; this study] and other continental regions worldwide [*Bell and Rossman*, 1992a; *Peslier et al.*, 2002; *Demouchy et al.*, 2006; *Grant et al.*, 2007b; *Li et al.*, 2008; *Bonadiman et al.*, 2009] are compiled in Figure 5. On the basis of the geodynamic position of their sources, peridotite xenoliths in other regions worldwide can be classified into two types: cratonic peridotite which is represented by South Africa and Colorado Plateau samples [*Bell and Rossman*, 1992a; *Grant et al.*, 2007b; *Li et al.*, 2008] and off-cratonic peridotite represented by Basin and Range (United States), Massif Central (France), Patagonia (Chile), and Antarctic samples [*Bell and Rossman*, 1992a; *Peslier et al.*, 2002; *Demouchy et al.*, 2006; *Grant et al.*, 2007b; *Li et al.*, 2008; *Bonadiman et al.*, 2009].

[32] Water contents of cpx of the NCC peridotites range between 5 and 355 ppm, with an average value of 108 ± 61 ppm; 85 out of 92 samples contain less than 200 ppm H_2O. In contrast, H_2O contents of cpx from the cratonic peridotites

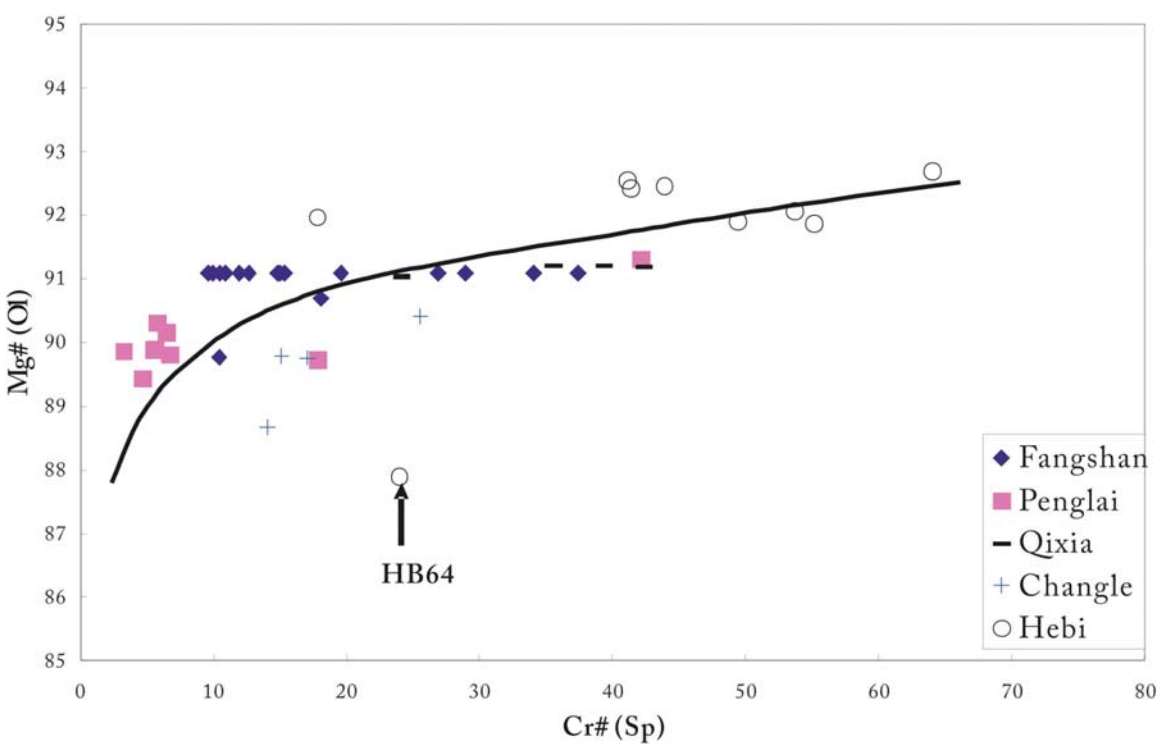

Figure 2. Mg # value of olivine versus Cr # value of spinel from Fangshan, Penglai, Qixia, Changle, and Hebi peridotite xenoliths of the NCC.

Table 5. Water Content, Mineral Mode, Temperature, Spinel $Fe^{3+}/\Sigma Fe$ and ΔFMQ of Peridotite Xenoliths Hosted by Cenozoic Basalts From the North China Craton[a]

Sample	Rock Type	Mode (%)				H_2O Content			T (°C)	ΔFMQ	Spinel $Fe^{3+}/\Sigma Fe$
		cpx	opx	ol	sp	cpx (ppm)	Opx (ppm)	WR (wt %)			
						Fangshan					
FS01	sp Lher	18	27	53	2	64	25	22	972	−1.0	0.11
FS03	sp Lher	13	27	58	2	167	68	50	1191		0.26
FS06	sp Lher	10	24	65	1	170	61	43	1044		0.18
FS07	sp Lher	12	28	57	3		60		1001	−0.6	0.17
FS11	sp Lher	9	21	69	1	109	43	26	998	2.2	0.29
FS12	sp Lher	7	30	61	2	158	54	37	1139		0.14
FS13	sp Lher	8	28	61	3	108	41	27	1092		0.17
FS14	sp Lher	11	20	66	3	120	53	32	1063		0.17
FS16	sp Lher	6	17	76	1	90	33	18	1023	−0.4	0.16
FS17	sp Lher	16	26	56	2	53	28	19	972	−1.5	0.09
FS18	sp Lher	9	20	70	1		63		1172	0.2	0.32
FS19	sp Lher	14	25	58	3		74		1113		0.22
FS21	sp Lher	10	20	68	2	177	69	44	1017		0.16
FS23	sp Lher	12	14	71	2	101	39	25	1094	0.6	0.25
FS24	sp Lher	16	34	48	1	41	21	16	928	0.3	0.22
FS26	sp Lher	9	20	70	1	67	28	16	967	−2.1	0.07
						Penglai					
PL01	sp Lher	9	27	62	2	52	24	14	924	0.5	0.20
PL10	sp Lher	6	20	72	2	53	16	10	932	0.9	0.24
PL17	sp Lher	7	19	72	2	48	19	10	903	0.9	0.20
PL19	sp Lher	12	18	67	3	35	17	10	918	0.9	0.22
PL32	sp Lher	10	13	76	1	49	14	10	945	0.3	0.20
PL36	sp Lher	10	22	65	3	59	21	14	903	1.4	0.26
PL42	sp Lher	8	16	75	1	48	25	11	942	0.0	0.16
PL44	sp Lher	11	15	72	2	48	11	10	914	−1.7	0.10
PL46	sp Lher	9	14	78	1	27	8	6	953	0.4	0.19
						Qixia					
QX01	sp Lher	6	23	68	3	70	32	16	951	−1.0	0.10
QX04	sp Lher	12	25	60	3	104	48	31	920	−4.2	0.02
QX14	sp Lher	8	20	70	2	158	52	34	925		
QX18	sp Lher	9	23	67	2	115	54	30	945	0.2	0.16
QX50	sp Lher	9	20	70	1	78	42	21	957	−0.1	0.14
QX51	sp Lher	18	20	61	1	158	59	50	883		
						Changle					
CL01	sp Lher	11	25	61	3	71	25	18	965		0.06
CL22	sp Lher	9	22	68	1	223	94	56	1010	−0.7	0.12
CL31	sp Lher	9	16	72	3	136	45	29	992	−1.2	0.11
CL32	sp Lher	10	16	73	1	111	25	23	934		
CL35	sp Harz	2	22	74	2		32		945		0.05
CL38	sp Lher	11	15	72	2	114	35	26	907		0.03
						Hebi					
HB02	sp Harz	<0.5	15	82	3		57	9	925	0.5	0.22
HB06	sp Harz	0	15	83	2		72	11	1056	0.2	0.21
HB07	sp Harz	0	20	78	2		52	10	798	0.6	0.17
HB10	sp Harz	0	25	73	2		72	18	760	1.2	0.27
HB12	sp Harz	0	18	80	2		96	17			0.22
HB16	sp Harz	0	15	84	1		64	10			0.16
HB17	sp Harz	<0.5	20	78	2		31	6	1057		0.18
HB64	sp Lher	10	10	77	3	181	86	41	1043	0.3	0.25
Average[b]						99 ± 51	44 ± 23	23 ± 13			
						Panshishan					
PSS01	sp Lher	10	18	71	1	95	26	21	960	−3.9	0.16
PSS02	sp Lher	15	20	65	1	129	30	34	956	−1.5	0.16
PSS05	sp Lher	12	20	62	2	161	34	36	964	−3.6	0.03
PSS07	sp Lher	15	31	52	2	147	30	39	971		0.08
PSS10	sp Lher	7	17	73	3		16		967		0.03
PSS11	sp Lher	12	29	57	2	103	26	26	888	0.0	0.32
PSS12	sp Lher	15	24	58	1	183	56	52	957	−4.1	0.09
PSS13	sp Lher	13	20	65	2	112	25	27	966		0.03
PSS15	sp Lher	10	26	62	3	64	17	15	902	0.3	0.25
PSS16	sp Lher	16	33	50	1	181	61	58	961		0.11
PSS17	sp Lher	5	18	75	2	177	50	31	953	−1.0	0.20
PSS18	sp Lher	15	22	60	3	121	23	31	861	−2.3	0.02
PSS19	sp Lher	13	16	70	1	145	23	33	959		
PSS20	sp Lher	12	27	59	2	150	23	33	902		

Table 5. (continued)

Sample	Rock Type	Mode (%)				H_2O Content			T (°C)	ΔFMQ	Spinel $Fe^{3+}/\Sigma Fe$
		cpx	opx	ol	sp	cpx (ppm)	Opx (ppm)	WR (wt %)			
						Lianshan					
LS01	sp Lher	10	21	67	2	55	18	13	924	0.0	0.08
LS02	sp Lher	23	26	49	2	41	13	15	907	−1.0	0.04
LS03	sp Lher	8	20	70	2	41	17	10	949	0.4	0.29
LS04	sp Lher	24	39	37		56	28	27	977	0.0	0.22
LS05	sp Lher	10	28	60	2	90	34	24	904		0.23
LS06	sp Lher	10	23	66	1	73	32	19	972	−0.6	0.08
LS07	sp Lher	12	27	60	1	96	30	26	967		0.20
LS08	sp Lher	14	27	57	2	42	15	12	931	−0.1	0.09
LS12	sp Lher	9	16	72	3	78	32	18	954	0.6	0.28
LS17	sp Lher	7	17	73	3	37	17	8	972	0.2	0.23
LS19	sp Lher	11	21	67	1	89	45	25	904	−0.4	0.07
LS20	sp Lher	10	10	78	2	84	34	18	966	−1.6	0.20
LS21	sp Lher	9	9	76	1		16	1		−2.5	0.05
LS22	sp Lher	12	22	64	2	102	41	28	914	−0.5	0.06
LS23	sp Lher	15	20	63	2	73	32	22	949	−1.1	0.11
LS24	sp Lher	15	28	56	1	80	34	26	950	−0.1	0.08
LS26	sp Lher	7	20	70	3	57	19	12	946	0.0	0.13
LS30	sp Lher	13	34	52	1	92	29	27	983	−0.7	0.10
LS31	sp Lher	16	15	68	1	55	16	15	893		0.06
						Hannuoba					
P1	sp Lher	9	18	71	2	85	25	18	866	−0.2	
P2	sp Lher	10	25	63	2	90	40	25	887	−1.3	0.16
P3	sp Lher	10	24	65	1	60	20	15	858	1.1	0.09
P4	sp Lher	5	18	74	3	50	20	10	1027	−0.1	0.34
P6	sp Lher	7	20	72	1	150	55	32	988	−0.3	0.18
P8	sp Lher	7	20	71	2	85	35	19	1006	−0.2	0.17
P11	sp Lher	9	15	75	1	70	35	17	992	−1.3	0.17
P12	sp Lher	13	20	65	2	110	35	28	969	−0.6	0.08
P13	sp Lher	15	27	55	3	100	45	33	915	−0.9	0.13
P14	sp Lher	9	25	65	1	140	55	35	857	−0.9	0.10
P15	sp Lher	7	23	68	2	125	55	30	947	0.1	0.11
P17	sp Lher	8	15	74	3	100	35	21	965		0.21
						Nushan					
NS01	sp Lher	9	25	64	1	190	105	56	913		
NS03	sp Lher	10	27	61	2	95	55	30	1099	−0.7	0.24
NS06	sp Lher	5	24	70	1	40	40	14	1084	−0.3	0.29
NS07	sp Lher	10	25	62	3	115	80	39	1107	−0.7	0.21
NS08	sp Harz	0	25	72	1		15	4	912	−0.4	0.29
NS12	sp Lher	7	28	63	2	165	110	53	1073		0.16
NS13	sp Lher	12	25	61	2	15	20	8	931	−1.4	0.12
NS14	sp Lher	18	30	51	1	215	95	78	1089		0.27
NS16	sp Lher	9	20	70	1	240	115	61	1090		0.09
NS21	sp Lher	9	22	65	2	215	90	53	937	−1.6	0.08
NS22	sp Lher	15	27	56	1	5	5	2	945	−3.4	0.09
NS24	sp Lher	18	25	55	2	245	110	85	1101	−1.7	0.14
NS25	sp Lher	7	18	73	2	355	140	76	1090		0.03
NS29	sp Lher	13	20	64	1	240	105	68	973		
NS30	sp Lher	5	16	75	1	55	40	13	899	−0.6	0.19
Average[c]						108 ± 61	42 ± 27	25 ± 18			

[a] H_2O content of cpx and opx of the Nushan and Hannuoba samples is from *Yang et al.* [2008]; that of Panshishan and Lianshan is from *Bonadiman et al.* [2009]. The whole-rock (WR) H_2O content were calculated by assuming Dcpx/ol as 10 to calculate olivine water content for all samples. Spinel $Fe^{3+}/\Sigma Fe$ and ΔFMQ of Nushan, Hannuoba, Panshishan, and Lianshan samples were calculated by this study (see text). Some samples have not calculated ΔFMQ values because of different two-pyroxene geothermometers differed by 200°C or more (see text). Temperature for all T estimates on the basis samples were estimated by the Ca-in-opx geothermometer of *Brey and Kohler* [1990]. Cpx, clinopyroxene; opx, orthopyroxene; ol, olivine; sp, spinel; Lher, lherzolite; Harz, harzburgite.

[b] Average value of the new samples from this study.

[c] Average value of all the NCC samples. Mineral modes are estimated by point-counting method on one to three thin sections.

range between 370 and 950 ppm with an average value of 577 ± 209 ppm (397 ± 61 ppm if slab-influenced Colorado Plateau samples [*Li et al.*, 2008] are excluded), while those of cpx from the off-cratonic peridotites range between 5 and 528 ppm with an average value of 316 ± 151 ppm (Figure 5a). H_2O contents of opx of the NCC peridotites range between 5 and 140 ppm, 96 out of 106 samples have less than 80 ppm and the average value is 42 ± 27 ppm. On the other hand, H_2O contents of opx from the cratonic peridotites range between 180 and 400 ppm, with an average value of 297 ± 94 ppm

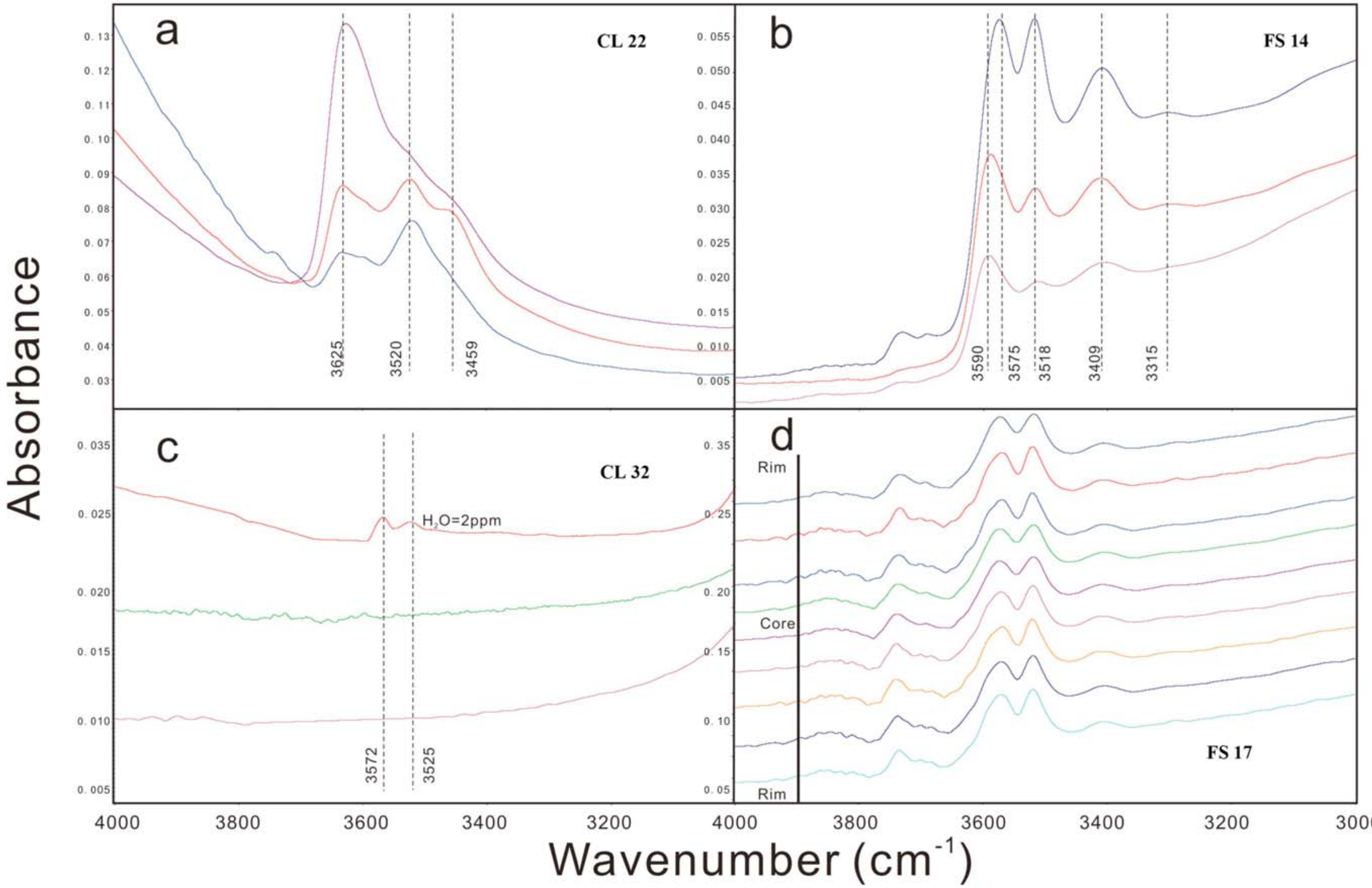

Figure 3. Representative IR spectra for (a) cpx, (b) opx, and (c) ol of the NCC peridotites. Spectra of three grains from the same peridotite are shown. (d) A profile analysis for an opx grain from one Fangshan peridotite (FS17). The absorption at 3740 cm^{-1} is an artifact of the instrument light; the weak 3710 cm^{-1} peak is possibly due to subtraction of a background spectrum slightly contaminated by the presence of water vapor. The H_2O content of one olivine grain from Changle (CL32) is calculated on the basis of the absorption coefficient of *Bell et al.* [2003]. For clarity, all spectra were offset vertically. The thickness is 0.31, 0.29, 0.34, and 0.28 mm for CL22, FS14, CL32, and FS17, respectively.

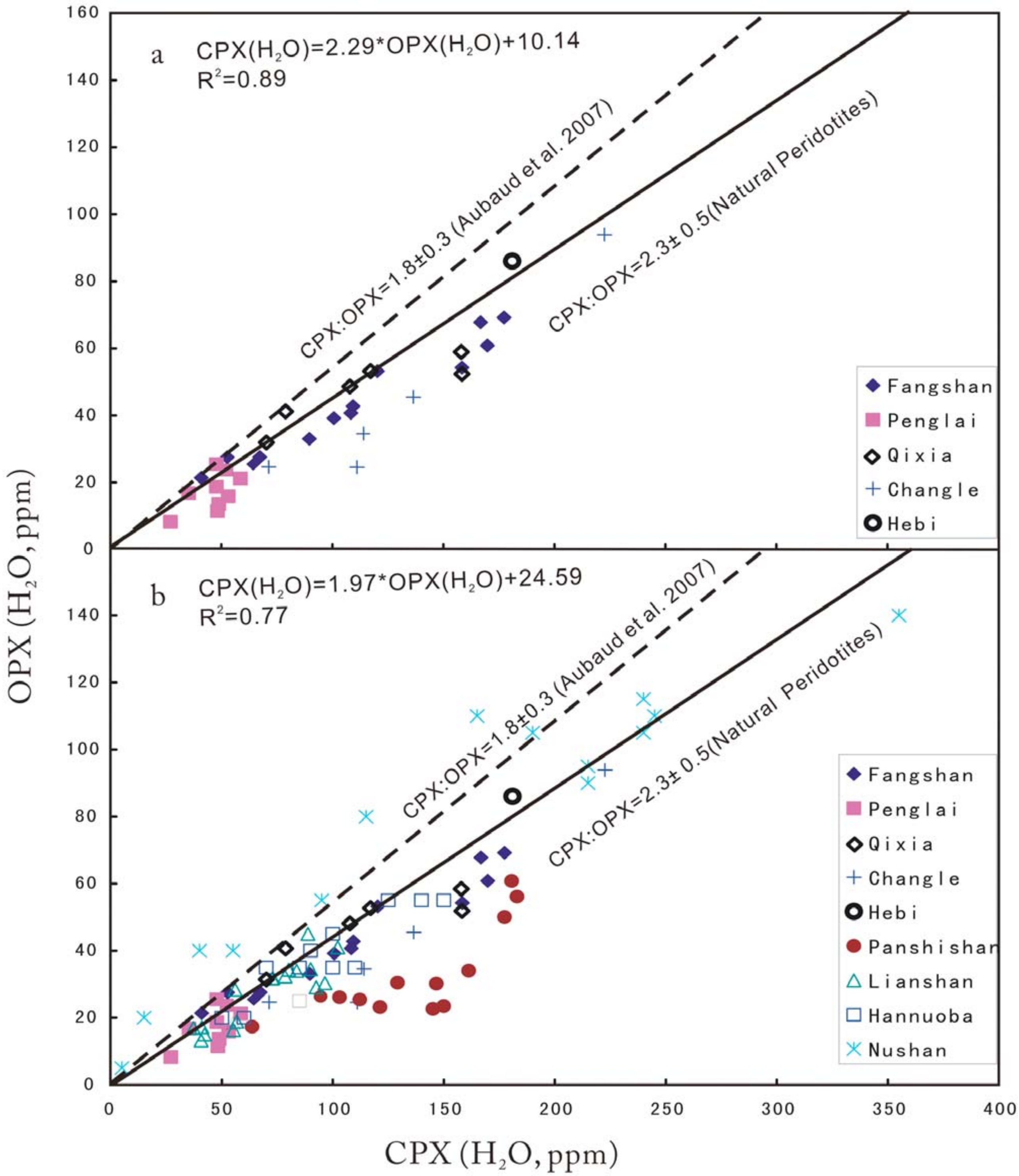

Figure 4. Opx H_2O content versus cpx H_2O content for peridotite xenoliths (a) from this study and (b) from this study and samples from Nushan and Hannuoba reported by *Aubaud et al.* [2007] and *Yang et al.* [2008] and Panshishan and Fangshan from *Bonadiman et al.* [2009]. The dashed lines represent the experimental partition coefficients obtained by *Aubaud et al.* [2007], and the solid lines are the partition coefficients for natural peridotite xenoliths (n = 38 [*Bell and Rossman*, 1992a; *Peslier et al.*, 2002; *Grant et al.*, 2007b; *Li et al.*, 2008]).

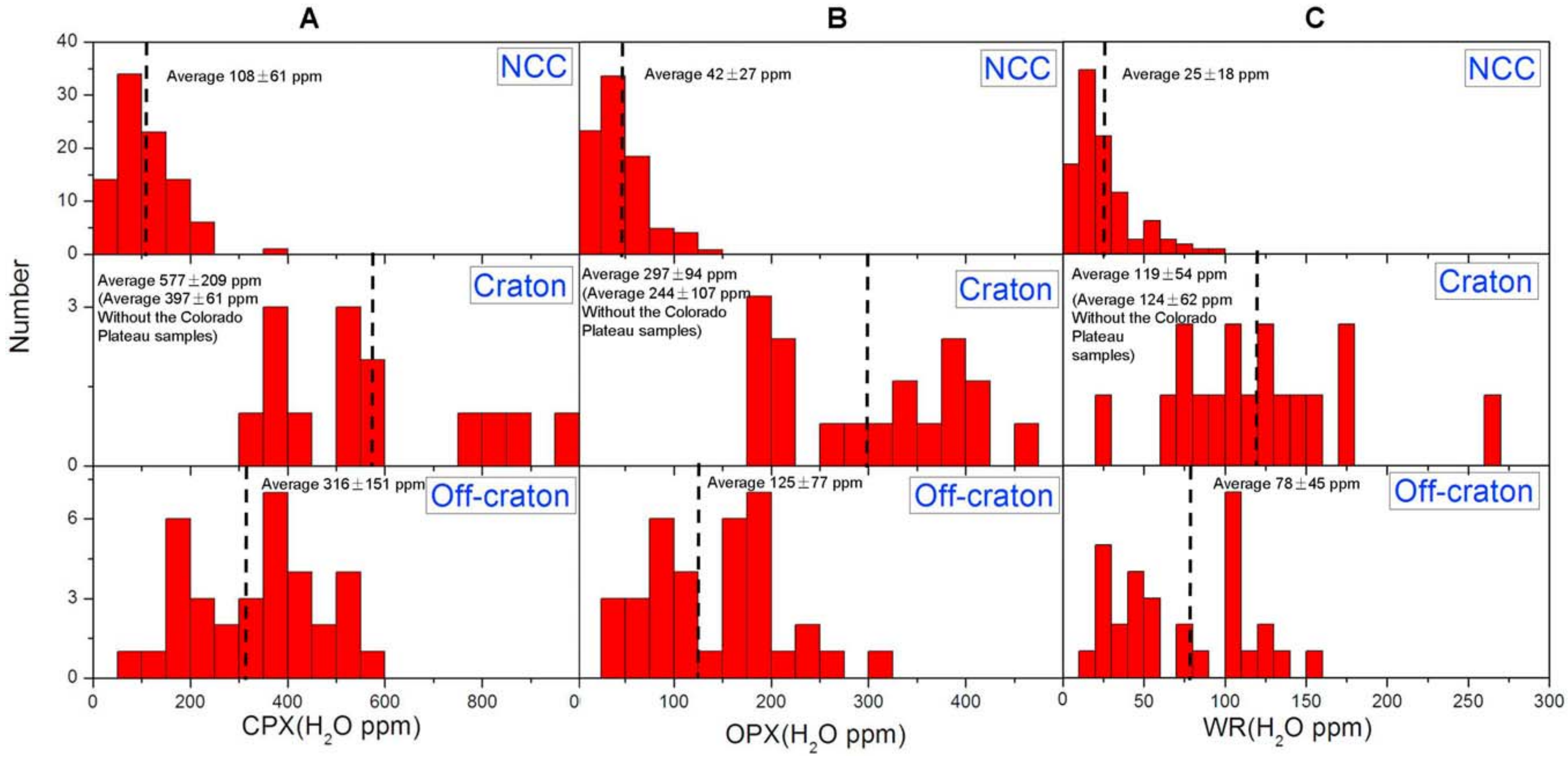

Figure 5. Comparison of H_2O contents of cpx, opx, and whole rock (WR) of the NCC peridotite xenoliths with those of cratonic and off-cratonic peridotites. The NCC data are from *Aubaud et al.* [2007] and *Yang et al.* [2008] for Nushan and Hannuoba, *Bonadiman et al.* [2009] for Panshishan and Lianshan, and this study for Fangshan, Penglai, Qixia, Changle, and Hebi. The data for cratonic peridotites (South Africa and Colorado Plateau) are from *Bell and Rossman* [1992a], *Grant et al.* [2007b], and *Li et al.* [2008]; the data for off-cratonic peridotites (Basin and Range area, French Massif Central, Patagonia, Antarctic and West Kettle, British Columbia) are from *Bell and Rossman* [1992a], *Peslier et al.* [2002], *Peslier and Luhr* [2006], *Demouchy et al.* [2006], *Grant et al.* [2007b], *Li et al.* [2008] and *Bonadiman et al.* [2009]. For cratonic samples, two average values are given: with or without the Colorado Plateau samples which were rehydrated by a subduction slab [*Li et al.*, 2008].

(244 ± 107 ppm if slab-influenced Colorado Plateau samples [*Li et al.*, 2008] are excluded), while those of opx from the off-cratonic peridotites range between 9 and 300 ppm, with an average value of 125 ± 77 ppm (Figure 5b).

[33] Comparison of whole rock values indicates a pattern consistent with the pyroxene data. The estimated whole rock water contents (calculating H_2O contents of ol by assuming Dcpx/ol = 10 for all the samples) of the NCC peridotite xenoliths range between 6 and 85 ppm with an average value of 25 ± 18 ppm. In contrast, those of cratonic peridotites are more than 60 ppm (except for one dunite from Colorado with 27 ppm) with an average value of 119 ± 54 ppm (124 ± 62 ppm if slab-influenced Colorado Plateau samples [*Li et al.*, 2008] are excluded). Those of off-cratonic peridotites are between 10 and 154 ppm, with an average value of 78 ± 45 ppm (Figure 5c).

[34] Only a few "off-craton" peridotites have water contents similar to those of NCC mantle xenoliths (Figure 6c). These harzburgite and dunite samples have experienced high degrees of partial melting [*Peslier et al.*, 2006; *Li et al.*, 2008; *Bonadiman et al.*, 2009]. As H_2O behaves as a highly incompatible element during partial melting of a mantle source [*Hauri et al.*, 2006; *Tenner et al.*, 2009], the peridotite residues undergoing higher degrees of partial melting are expected to be more depleted in water. Moreover, lherzolites from San Carlos Cenozoic basalts have low water contents (171 to 178 ppm for cpx, 53 to 82 ppm for opx, and 2 to 4 ppm for ol [*Li et al.*, 2008]) similar to those of the NCC lherzolites. The low water contents of these rocks have been interpreted to result from water loss during partial melting [*Li et al.*, 2008].

5.2.2. Comparison With the Oceanic Mantle

[35] The available data for oceanic peridotites are very scarce. *Peslier et al.* [2007] analyzed three abyssal peridotites from Gakkel ridge, Arctic Ocean; the H_2O contents are <1–5 ppm for ol, 25–60 ppm for opx, and 130–200 ppm for cpx. The low water contents of these samples are likely the consequence of water loss during the slow adiabatic decompression; thus they do not necessarily represent the mid-oceanic basalt (MORB). *Gose et al.* [2009b] investigated a suite of abyssal peridotites from the Mid-Atlantic Ridge. The measured H_2O contents of opx range between 160 and 270 ppm and are suggested to reflect the original mantle contents. This range is much higher than that of opx of the NCC peridotites which varied from 5 to 140 ppm (96 out of 106 samples have water contents <80 ppm; Figure 5b).

[36] In contrast to oceanic peridotites, the H_2O contents of MORB and OIB have been well constrained from melt inclusions and glass [*Dixon et al.*, 1988, 1997, 2002; *Michael*, 1988, 1995; *Stolper and Newmann*, 1994; *Sobolev and Chaussidon*, 1996; *Danyushevsky et al.*, 2000; *Nichols et al.*, 2002; *Saal et al.*, 2002; *Simons et al.*, 2002; *Wallace et al.*, 2002; *Asimow et al.*, 2004; *Seaman et al.*, 2004; *Workman et al.*, 2006]. On the basis of these data, the H_2O contents of the sources of MORB and OIB are calculated to be about 50 to 250 ppm [*Dixon et al.*, 1988; *Michael*, 1988; *Sobolev and Chaussidon*, 1996; *Saal et al.*, 2002; *Simons et al.*, 2002; *Asimow et al.*, 2004] and between 300 and 1000 ppm, respectively [*Dixon et al.*, 1997; *Wallace et al.*, 2002; *Nichols et al.*, 2002; *Simons et al.*, 2002; *Seaman et al.*, 2004; *Workman et al.*, 2006]. Consequently, the H_2O contents of the NCC peridotites are lower than those of the oceanic mantle represented by the sources of MORB and OIB.

5.3. Possible Role of Redox State on Water Content

[37] On the basis of the negative correlation between water content of pyroxenes and oxygen fugacity for Mexican and Simcoe (Washington) spinel peridotite xenoliths, *Peslier et al.* [2002] suggested that pyroxene water contents are mainly controlled by the redox state of peridotites. In order to test this model in the NCC peridotites, we calculated the spinel $Fe^{3+}/\Sigma Fe$ ratio and the peridotite oxygen fugacity (expressed as variation relative to the fayalite-magnetite-quartz oxygen buffer or ΔFMQ) based on EMP data from *Yang et al.* [2008] and from this study. Fe^{3+} values for spinels were calculated following the equation: $Fe^{3+} = 8 - (4Ti + 3Al + 3Cr + 2Fe + 2Mn + 2Ni + 2Mg)$ using atomic formula units normalized to three cations and discarding negative values. ΔFMQ values were calculated following the protocol of *Woodland et al.* [1992]. A pressure of 15 kbar was assumed for all the samples. If the temperature estimates from two opx-cpx thermometers [*Wells*, 1977; *Brey and Kohler*, 1990] differed by 200°C or more, the samples were discarded for ΔFMQ calculation. The overall uncertainty was empirically estimated to be ±0.5 log units. The spinel $Fe^{3+}/\Sigma Fe$ ratios and ΔFMQ values are given in Table 5. ΔFMQ values for the NCC peridotites vary from −4.2 to +2.2, with most ranging between −2.5 and +0.5. These values fall in the range of continental mantle as represented by peridotite xenoliths and peridotite massifs [*Frost and McCammon*, 2008, and references therein]. Spinel $Fe^{3+}/\Sigma Fe$ values of the NCC peridotites vary from 0.03 to 0.34, with most values between 0.10 to 0.34, in the range of continental spinel peridotites (most of them range from 0.15 to 0.34 [*Frost and McCammon*, 2008, and references therein]) and the Mexican and Simcoe spinel peridotites [*Peslier et al.*, 2002]. Some of the NCC spinels have low $Fe^{3+}/\Sigma Fe$ values, down to 0.03, and the majority of the NCC peridotites are not characterized by oxidized signatures (ΔFMQ > 0). In addition, no correlation between pyroxene H_2O content and spinel $Fe^{3+}/\Sigma Fe$ and peridotite ΔFMQ values can be observed (Figure 6). Therefore, the low water content of the NCC samples cannot be related to high oxygen fugacity as has been argued in the case of the Simcoe peridotites [*Peslier et al.*, 2002].

5.4. Implications of the Low Water Content of the Eastern NCC

[38] The mechanisms responsible for lithospheric thinning of the NCC have been extensively debated [*Menzies and Xu*, 1998; *Griffin et al.*, 1998; *Zheng et al.*, 1998, 2001, 2006; *Xu,* 2001, *Y. G. Xu et al.*, 2008; *Gao et al.*, 2002, 2004, 2008; *Zhang et al.*, 2002, 2008, 2009; *Zhang*, 2005; *Wu et al.*, 2003, 2006; *Niu*, 2005; *Menzies et al.*, 2007]. Several models have been proposed, which can be grouped into two end-members: "top-down" rapid (<10 Ma) delamination models versus "bottom-up" protracted (possibly up to 100 Ma) thermomechanical-chemical erosion models. Delamination would have produced the removal of the entire lithospheric mantle and probably part of the lower crust [*Wu et al.*, 2003, 2006; *Gao et al.*, 2004, 2008]. Thus the resulting (present) lithospheric mantle beneath the NCC would be asthenospheric mantle, newly accreted and cooled during the late Mesozoic-early Cenozoic thinning. On the other hand,

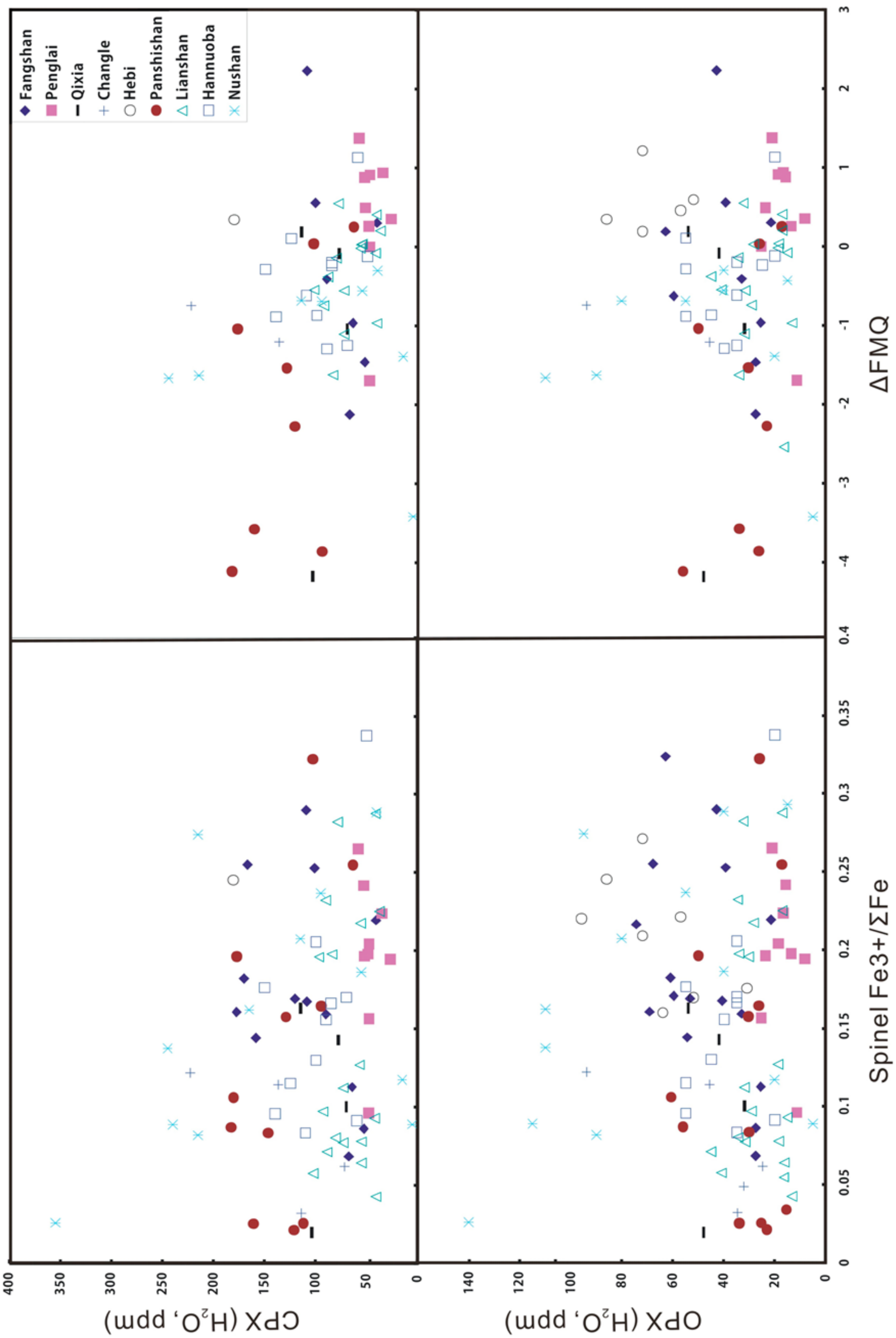

Figure 6. H_2O content of cpx and opx versus $Fe^{3+}/\Sigma Fe$ of spinel and ΔFMQ of peridotite from the NCC.

thermal erosion models predict that most of the present lithospheric mantle is composed of thinned, relict Archean-Proterozoic mantle [*Griffin et al.*, 1998; *Menzies and Xu*, 1998; *Xu*, 2001].

[39] According to the delamination model, the newly formed lithospheric mantle should be composed of essentially unmodified, cooled asthenosphere because there was no significant asthenosphere-derived basaltic magmatism associated with the NCC lithospheric thinning [*Menzies et al.*, 2007, and references therein]. If the delamination model is accepted, the water contents of the present lithospheric mantle should be similar to that of the source of MORB (50–250 ppm), which is not the case for the majority of the eastern NCC peridotites. Moreover, the fact that the NCC peridotites display water contents much lower than those of oceanic peridotites from the Mid-Atlantic Ridge [*Gose et al.*, 2009b] also argues against an asthenospheric source.

[40] Therefore, we suggest that the low water contents of the eastern NCC samples result from the reheating of the lithosphere from below by an upwelling asthenospheric flow that occurred in concert with lithospheric thinning. If so, most of the Cenozoic lithospheric mantle of the eastern NCC should be considered as relict ancient mantle after lithospheric thinning during the late Mesozoic-early Cenozoic. A few peridotite xenoliths from Nushan and Changle (Table 5) having H_2O content greater than 50 ppm (up to 85 ppm) may actually represent newly accreted and cooled asthenospheric materials. This scenario is in agreement with the available age constraints from Re-Os isotopic data on peridotite xenoliths hosted by Cenozoic basalts from the eastern NCC (including whole rock and sulfides) [*Meisel et al.*, 2001; *Gao et al.*, 2002; *Xia et al.*, 2004; *Reisberg et al.*, 2005; *Wu et al.*, 2006; *Zhi et al.*, 2007; *Y. G. Xu et al.*, 2008; *X. S. Xu et al.*, 2008; *Zhang et al.*, 2009]. Using the Os proxy isochron ($^{187}Os/^{188}Os$ versus Al_2O_3 or Yb, etc.), the melting age of the eastern NCC lithospheric mantle is early Proterozoic to Mesoproterozoic. Taking into consideration the Re depletion model ages (T_{RD}) of the most depleted samples of each area, we also obtain a Proterozoic age, which represents a minimum age for melt extraction.

6. Conclusions

[41] 1. The H_2O contents of cpx, opx and ol of peridotite xenoliths hosted by Cenozoic basalts from the eastern part of the NCC (Fangshan, Penglai, Qixia, Changle, and Hebi) are 27–223 ppm, 8–94 ppm, and ~0 ppm respectively. The homogenous H_2O distributions within single pyroxene grains and the equilibrium partitioning of H_2O between cpx and opx support the proposition that the pyroxenes largely preserve their initial H_2O contents, acquired in their mantle source. The recalculated whole-rock H_2O contents, using mineral modes and assuming a partition coefficient of 10 for water between cpx and ol, range from 6 to 56 ppm, with an average of 23 ± 13 ppm.

[42] 2. In combination with previously reported data [*Yang et al.*, 2008; *Bonadiman et al.*, 2009], the whole rock water contents of peridotite xenoliths (105 samples from 9 localities) hosted by Cenozoic basalts from the eastern part of the NCC range from 6 to 85 ppm (average: 25 ± 18 ppm). The Cenozoic lithospheric mantle of the eastern part of the NCC is therefore characterized by a low water content compared to worldwide continental lithospheric mantle represented by typical cratonic and off-cratonic peridotites (most of them range between 40 and 180 ppm, with average values of 119 ± 54 ppm and 78 ± 45 respectively) and to oceanic mantle (>50 ppm H_2O inferred for the sources of MORB and OIB). This low water content is not related to the oxygen fugacity. We speculate that the low water content resulted from reheating by upwelling asthenospheric flow accompanying late Mesozoic to early Cenozoic lithospheric thinning. If this hypothesis is correct, the present eastern NCC lithospheric mantle mostly represents thinned, relict Archean-Proterozoic lithospheric mantle, rather than newly accreted, cooled asthenospheric mantle.

[43] **Acknowledgments.** We thank Anne Peslier and an anonymous reviewer for their thorough and very helpful reviews and the AE for editorial handling and valuable comments. We are indebted to Jannick Ingrin and Laurie Reisberg for revising the manuscript and improving English. This work was supported by the National Science Foundation of China (90714009) and China-France-Italy cooperative project.

References

Arai, S. (1994), Characterization of spinel peridotites by olivine-spinel compositional relationships: Review and interpretation, *Chem. Geol.*, *113*, 191–204, doi:10.1016/0009-2541(94)90066-3.

Asimow, P. D., J. E. Dixon, and C. H. Langmuir (2004), A hydrous melting and fractionation model for mid-ocean ridge basalts: Application to the Mid-Atlantic Ridge near the Azores, *Geochem. Geophys. Geosyst.*, *5*, Q01E16, doi:10.1029/2003GC000568.

Asimow, P. D., L. C. Stein, J. L. Mosenfelder, and G. R. Rossman (2006), Quantitative polarized infrared analysis of trace OH in populations of randomly oriented mineral grains, *Am. Mineral.*, *91*, 278–284, doi:10.2138/am.2006.1937.

Aubaud, C., E. H. Hauri, and M. M. Hirschmann (2004), Hydrogen partition coefficients between nominally anhydrous minerals and basaltic melts, *Geophys. Res. Lett.*, *31*, L20611, doi:10.1029/2004GL021341.

Aubaud, C., A. C. Withers, M. M. Hirschmann, Y. Guan, L. A. Leshin, S. Mackwell, and D. R. Bell (2007), Intercalibration of FTIR and SIMS for hydrogen measurements in glasses and nominally anhydrous minerals, *Am. Mineral.*, *92*, 811–828, doi:10.2138/am.2007.2248.

Bell, D. R., and G. R. Rossman (1992a), Water in the Earth's mantle: The role of nominally anhydrous minerals, *Science*, *255*, 1391–1397, doi:10.1126/science.255.5050.1391.

Bell, D. R., and G. R. Rossman (1992b), The distribution of hydroxyl in garnets from the subcontinental mantle of southern Africa, *Contrib. Mineral. Petrol.*, *111*, 161–178, doi:10.1007/BF00348949.

Bell, D. R., P. D. Ihinger, and G. R. Rossman (1995), Quantitative analysis of hydroxyl in garnet and pyroxene, *Am. Mineral.*, *80*, 465–474.

Bell, D. R., G. R. Rossman, J. Maldener, D. Endisch, and F. Rauch (2003), Hydroxide in olivine: A quantitative determination of the absolute amount and calibration of the IR spectrum, *J. Geophys. Res.*, *108*(B2), 2105, doi:10.1029/2001JB000679.

Bell, D. R., G. R. Rossman, and R. O. Moore (2004), Abundance and partitioning of OH in a high-pressure magmatic system megacrysts from the Monastery Kimberlite, South Africa, *J. Petrol.*, *45*, 1539–1564, doi:10.1093/petrology/egh015.

Bernstein, S., P. B. Kelemen, and K. Hanghøj (2007), Consistent olivine Mg# in cratonic mantle reflects Archean mantle melting to the exhaustion of orthopyroxene, *Geology*, *35*, 459–462, doi:10.1130/G23336A.1.

Berry, A. J., J. Hermann, H. S. C. O'Neill, and G. J. Foran (2005), Fingerprinting the water site in mantle olivine, *Geology*, *33*, 869–872, doi:10.1130/G21759.1.

Bonadiman, C., Y. T. Hao, M. Coltorti, L. Dallai, B. Faccini, Y. Huang, and Q. K. Xia (2009), Water contents in pyroxenes from intraplate lithospheric mantle, *Eur. J. Mineral.*, *21*, 637–647, doi:10.1127/0935-1221/2009/0021-1935.

Brey, G. P., and T. Kohler (1990), Geothermobarometry in four-phase lherzolites: II. New thermo-barometers and practical assessment of existing thermobarmeters, *J. Petrol.*, *31*, 1353–1378.

Carpenter, W. S., S. Mackwell, and D. Dyar (2000), Hydrogen in diopside: Diffusion profiles, *Am. Mineral.*, *85*, 480–487.

Chen, D. G., and Z. C. Peng (1988), K-Ar ages and Pb, Sr isotopic characteristics of some Cenozoic volcanic rocks from Anhui and Jiangsu provinces, China (in Chinese), *Acta Petrol. Sin.*, *4*, 3–12.

Chen, S. H., S. Y. O'Reilly, X. H. Zhou, W. L. Griffin, G. H. Zhang, M. Sun, J. L. Feng, and M. Zhang (2001), Thermal and petrological structure of the lithosphere beneath Hannuoba, Sino-Korean craton, China: Evidence from xenoliths, *Lithos*, *56*, 267–301, doi:10.1016/S0024-4937(00)00065-7.

Danyushevsky, L. V., S. M. Eggins, T. J. Falloon, and D. M. Christie (2000), H_2O abundances in depleted to moderately enriched mid-ocean ridge magma, 1: Incompatible behavior, implications for mantle storage, and origins of regional variations, *J. Petrol.*, *41*, 1329–1364, doi:10.1093/petrology/41.8.1329.

Demouchy, S., S. D. Jacobsen, F. Gaillard, and C. R. Stern (2006), Rapid magma ascent recorded by water diffusion profiles in olivine from Earth's mantle, *Geology*, *34*, 429–432, doi:10.1130/G22386.1.

Dixon, J. E., E. Stolper, and J. R. Delany (1988), Infrared spectroscopic measurements of CO_2 and H_2O in Jun de Fuca Ridge basaltic glasses, *Earth Planet. Sci. Lett.*, *90*, 87–104, doi:10.1016/0012-821X(88)90114-8.

Dixon, J. E., D. A. Clague, P. Wallace, and R. Poreda (1997), Volatiles in alkali basalts from the North Arch Volcanic Field, Hawaii: Extensive degassing of deep submarine-erupted alkalic series lavas, *J. Petrol.*, *38*, 911–939, doi:10.1093/petrology/38.7.911.

Dixon, J. E., L. Leist, C. Langmuir, and J. G. Schilling (2002), Recycled dehydrated lithosphere observed in plume-influenced mid-ocean-ridge basalt, *Nature*, *420*, 385–389, doi:10.1038/nature01215.

Fan, Q. C., and P. R. Hooper (1989), The mineral chemistry of ultramafic xenoliths of Eastern China-implications for upper mantle composition and paleogeotherms, *J. Petrol.*, *30*, 1117–1158.

Fan, W. M., H. F. Zhang, J. Baker, K. E. Jarvis, P. R. D. Mason, and M. A. Menzies (2000), On and off the North China Craton: Where is the Archean keel?, *J. Petrol.*, *41*, 933–950, doi:10.1093/petrology/41.7.933.

Frost, D. J., and C. A. McCammon (2008), The redox state of Earth's mantle, *Annu. Rev. Earth Planet. Sci.*, *36*, 389–420, doi:10.1146/annurev.earth.36.031207.124322.

Gao, S., R. L. Rudnick, R. W. Carlson, W. F. McDonough, and Y. S. Liu (2002), Re-Os evidence for replacement of ancient mantle lithosphere beneath the North China Craton, *Earth Planet. Sci. Lett.*, *198*, 307–322, doi:10.1016/S0012-821X(02)00489-2.

Gao, S., R. L. Rudnick, H. L. Yuan, X. M. Liu, Y. S. Liu, W. L. Xu, W. Ling, J. Ayers, X. C. Wang, and Q. H. Wang (2004), Recycling lower continental crust in the North China Craton, *Nature*, *432*, 892–897, doi:10.1038/nature03162.

Gao, S., et al. (2008), Recycling deep cratonic lithosphere and generation of intraplate magmatism in the North China Craton, *Earth Planet. Sci. Lett.*, *270*, 41–53, doi:10.1016/j.epsl.2008.03.008.

Gaul, O. F., W. L. Griffin, S. Y. O'Reilly, and N. J. Pearson (2000), Mapping olivine composition in the lithospheric mantle, *Earth Planet. Sci. Lett.*, *182*, 223–235, doi:10.1016/S0012-821X(00)00243-0.

Gose, J., P. Reichart, G. Dollinger, and E. Schmädicke (2009a), Water in natural olivine—Determined by proton-proton scattering analysis, *Am. Mineral.*, *93*, 1613–1619, doi:10.2138/am.2008.2835.

Gose, J., E. Schmädicke, and A. Beran (2009b), Water in enstatite from Mid-Atlantic Ridge peridotite: Evidence for the water content of suboceanic mantle?, *Geology*, *37*, 543–546, doi:10.1130/G25558A.1.

Grant, K. J., S. C. Kohn, and R. A. Brooker (2007a), The partitioning of water between olivine, orthopyroxene and melt synthesized in the system albite-forsterite-H_2O, *Earth Planet. Sci. Lett.*, *260*, 227–241, doi:10.1016/j.epsl.2007.05.032.

Grant, K. J., J. Ingrin, J. P. Lorland, and P. Dumas (2007b), Water partition between mantle minerals from peridotite xenoliths, *Contrib. Mineral. Petrol.*, *154*, 15–34, doi:10.1007/s00410-006-0177-1.

Griffin, W. L., A. D. Zhang, S. Y. O'Reilly, and C. G. Ryan (1998), Phanerozoic evolution of the lithosphere beneath the Sino-Korean Craton, in *Mantle Dynamics and Plate Interactions in East Asia, Geodyn. Ser.*, vol. 27, edited by M. F. J. Flower et al., pp. 107–126, AGU, Washington, D. C.

Hauri, E. H., G. A. Gaetani, and T. H. Green (2006), Partitioning of water during melting of the Earth's upper mantle at H_2O-undersaturated conditions, *Earth Planet. Sci. Lett.*, *248*, 715–734, doi:10.1016/j.epsl.2006.06.014.

Hercule, S., and J. Ingrin (1999), Hydrogen in diopside: Diffusion, kinetics of extraction-incorporation, and solubility, *Am. Mineral.*, *84*, 1577–1587.

Hier-Majumder, S., S. Mei, and D. L. Kohlstedt (2005), Water weakening of clinopyroxeneite in diffusion creep, *J. Geophys. Res.*, *110*, B07406, doi:10.1029/2004JB003414.

Hirschmann, M. M., C. Aubaud, and A. C. Withers (2005), Storage capacity of H_2O in nominally anhydrous minerals in the upper mantle, *Earth Planet. Sci. Lett.*, *236*, 167–181, doi:10.1016/j.epsl.2005.04.022.

Hirschmann, M. M., T. Tenner, C. Aubaud, and A. C. Withers (2009), Dehydration melting of nominally anhydrous mantle: The primacy of partitioning, *Phys. Earth Planet. Inter.*, *176*, 54–68, doi:10.1016/j.pepi.2009.04.001.

Hirth, G., and D. L. Kohlstedt (1996), Water in the oceanic upper mantle: Implications for rheology, melt extraction and the evolution of the lithosphere, *Earth Planet. Sci. Lett.*, *144*, 93–108, doi:10.1016/0012-821X(96)00154-9.

Ingrin, J., and H. Skogby (2000), Hydrogen in nominally anhydrous upper-mantle minerals: Concentration levels and implications, *Eur. J. Mineral.*, *12*, 543–570.

Jaques, A. L., and G. H. Green (1980), Anhydrous melting of peridotite at 0–15 kb pressure and the genesis of tholeiitic basaltic magma, *Contrib. Mineral. Petrol.*, *73*, 287–310, doi:10.1007/BF00381447.

Jin, L. Y. (1985), K-Ar ages of Cenozoic volcanic rocks in the middle segment of the Tancheng-Lujiang Fault Zone and stages of related volcanic activity (in Chinese), *Geol. Rev.*, *31*, 309–315.

Karato, S., and H. Jung (1998), Water, partial melting and the origin of seismic low velocity and high attenuation zone in the upper mantle, *Earth Planet. Sci. Lett.*, *157*, 193–207, doi:10.1016/S0012-821X(98)00034-X.

Keppler, H., and N. Bolfan-Casanova (2006), Thermodynamics of water solubility and partitioning, in *Water in Nominally Anhydrous Minerals, Rev. Mineral. Geochem.*, vol. 62, edited by H. Keppler and J. R. Smyth, pp. 193–230, Mineral. Soc. of Am., Washington, D. C.

Koga, K., E. Hauri, M. M. Hirschmann, and D. R. Bell (2003), Hydrogen concentration analyses using SIMS and FTIR: Comparison and calibration for nominally anhydrous minerals, *Geochem. Geophys. Geosyst.*, *4*(2), 1019, doi:10.1029/2002GC000378.

Kohlstedt, D. L., and S. J. Mackwell (1998), Diffusion of hydrogen and intrinsic point defects in olivine, *Z. Phys. Chem.*, *307*, 147–162.

Kovacs, I., J. Hermann, H. S. C. O'Neill, J. F. Gerald, M. Sambridge, and G. Horvath (2008), Quantitative absorbance spectroscopy with unpolarized light: Part II. Experimental evaluation and development of a protocol for quantitative analysis of mineral IR spectra, *Am. Mineral.*, *93*, 765–778, doi:10.2138/am.2008.2656.

Li, Z. X., C. A. Lee, A. H. Peslier, A. Lenard, and S. J. Mackwell (2008), Water contents in mantle xenoliths from the Colorado Plateau and vicinity: Implications for the mantle rheology and hydration-induced thinning of continental lithosphere, *J. Geophys. Res.*, *113*, B09210, doi:10.1029/2007JB005540.

Liu, D. Y., A. P. Nutman, W. Compston, J. S. Wu, and Q. H. Shen (1992), Remnants of 3800 Ma crust in the Chinese part of the Sino-Korean craton, *Geology*, *20*, 339–342, doi:10.1130/0091-7613(1992)020<0339:ROMCIT>2.3.CO;2.

Liu, R., W. Chen, J. Sun, and D. Li (1990), The K-Ar age and tectonic environment of Cenozoic volcanic rock in China, in *The Age and Geochemistry of Cenozoic Volcanic Rocks in China*, edited by R. Liu, pp. 1–43, Seismol. Publ. House, Beijing.

Meisel, T., R. L. Walker, and A. J. Irving (2001), Osmium isotopic compositions of mantle xenoliths: A global perspective, *Geochim. Cosmochim. Acta*, *65*, 1311–1323, doi:10.1016/S0016-7037(00)00566-4.

Menzies, M. A., and Y. G. Xu (1998), Geodynamics of the North China Craton, in *Mantle Dynamics and Plate Interactions in East Asia, Geodyn. Ser.*, vol. 27, edited by M. F. J. Flower et al., pp. 155–165, AGU, Washington, D. C.

Menzies, M. A., W. M. Fan, and M. Zhang (1993), Palaeozoic and Cenozoic lithoprobes and the loss of >120 km of Archaean lithosphere, Sino-Korean craton, China, in Magmatic Processes and Plate Tectonics, edited by H. M. Prichard, T. Alabaster, and C. R. Neary, *Geol. Soc. Spec. Publ.*, *76*, 71–81, doi:10.1144/GSL.SP.1993.076.01.04.

Menzies, M. A., Y. G. Xu, H. F. Zhang, and W. M. Fan (2007), Integration of geology, geophysics and geochemistry: A key to understanding the North China Craton, *Lithos*, *96*, 1–21, doi:10.1016/j.lithos.2006.09.008.

Michael, P. (1988), The concentration, behavior and storage of H_2O in the suboceanic upper mantle: Implications for mantle metasomatism, *Geochim. Cosmochim. Acta*, *52*, 555–566, doi:10.1016/0016-7037(88)90110-X.

Michael, P. J. (1995), Regionally distinctive sources of depleted MORB: Evidence from trace elements and H_2O, *Earth Planet. Sci. Lett.*, *131*, 301–320, doi:10.1016/0012-821X(95)00023-6.

Mierdel, K., H. Keppler, J. R. Smyth, and F. Langenhorst (2007), Water solubility in aluminous orthopyroxene and the origin of earth's asthenosphere, *Science*, *315*, 364–368, doi:10.1126/science.1135422.

Nichols, A. R. L., M. R. Carroll, and A. Hoskuldsson (2002), Is the Iceland hot spot also wet? Evidence from the water contents of undegassed submarine and subglacial pillow basalts, *Earth Planet. Sci. Lett.*, *202*, 77–87, doi:10.1016/S0012-821X(02)00758-6.

Niu, Y. (2005), Generation and evolution of basaltic magmas: Some basic concepts and a hypothesis for the origin of the Mesozoic-Cenozoic volcanism in eastern China, *Geol. J. China Univ.*, *11*, 9–46.

Paterson, M. S. (1982), The determination of hydroxyl by infrared-absorption in quartz, silicate-glasses and similar materials, *Bull. Mineral.*, *105*, 20–29.

Peslier, A. H. (2010), A review of water contents of nominally anhydrous natural minerals in the mantles of Earth, Mars and the Moon, *J. Volcanol. Geotherm. Res.*, doi:10.1016/j.volgeores.2009.10.006, in press.

Peslier, A. H., and J. F. Luhr (2006), Hydrogen loss from olivines in mantle xenoliths from Simcoe (USA) and Mexico: Mafic alkalic magma ascent rates and water budget of the sub-continental lithosphere, *Earth Planet. Sci. Lett.*, *242*, 302–319, doi:10.1016/j.epsl.2005.12.019.

Peslier, A. H., J. F. Luhr, and J. Post (2002), Low water contents on pyroxenes from spinel-peridotite of the oxidized, sub-arc mantle wedge, *Earth Planet. Sci. Lett.*, *201*, 69–86, doi:10.1016/S0012-821X(02)00663-5.

Peslier, A. H., J. E. Snow, E. Hellebrand, and A. Von Der Handt (2007), Low water contents in minerals from Gakkel ridge abyssal peridotites, Arctic Ocean, paper presented at 17th V. M. Goldschmidt Conference, Geochem. Soc., Cologne, Germany.

Peslier, A. H., A. B. Woodland, and J. A. Wolff (2008), Fast kimberlite ascent rates estimated from hydrogen diffusion profiles in xenolithc olivines from South Africa, *Geochim. Cosmochim. Acta*, *72*, 2711–2722, doi:10.1016/j.gca.2008.03.019.

Reisberg, L., X. C. Zhi, J. P. Lorang, Z. C. Peng, and C. Zimmermann (2005), Re-Os and S systematics of spinel peridotite xenoliths from east central China: Evidence for contrasting effects of melt percolation, *Earth Planet. Sci. Lett.*, *239*, 286–308, doi:10.1016/j.epsl.2005.09.010.

Rudnick, R. L., S. Gao, W. L. Ling, Y. S. Liu, and W. F. McDonough (2004), Petrology and geochemistry of spinel peridotite xenoliths from Hannuoba and Qixia, North China Craton, *Lithos*, *77*, 609–637, doi:10.1016/j.lithos.2004.03.033.

Saal, A., E. H. Hauri, C. H. Langmuir, and M. Perfit (2002), Vapor undersaturation in primitive mid-ocean ridge basalt and the volatile content of the Earth's upper mantle, *Nature*, *419*, 451–455, doi:10.1038/nature01073.

Seaman, C., S. B. Sherman, M. O. Garcia, M. B. Baker, B. Balta, and E. Stolper (2004), Volatiles in glasses from the HSDP2 drill core, *Geochem. Geophys. Geosyst.*, *5*, Q09G16, doi:10.1029/2003GC000596.

Simons, K., J. E. Dixon, J.-G. Schilling, R. Kingsley, and R. Poreda (2002), Volatiles in basaltic glasses from the Easter-Salas y Gomez Seamount Chain and Easter Microplate: Implications for geochemical cycling of volatile elements, *Geochem. Geophys. Geosyst.*, *3*(7), 1039, doi:10.1029/2001GC000173.

Skogby, H., and G. R. Rossman (1989), OH in pyroxene: An experimental study of incorporation mechanisms and stability, *Am. Mineral.*, *74*, 1059–1069.

Skogby, H., D. R. Bell, and G. R. Rossman (1990), Hydroxide in pyroxene: Variations in the natural environment, *Am. Mineral.*, *75*, 764–774.

Sobolev, A. V., and M. Chaussidon (1996), H_2O concentrations in primary melts from supra-subduction zones and mid-ocean ridges: Implications for H_2O storage and recycling in the mantle, *Earth Planet. Sci. Lett.*, *137*, 45–55, doi:10.1016/0012-821X(95)00203-O.

Stalder, R., and H. Skogby (2003), Hydrogen diffusion in natural and synthetic orthopyroxene, *Phys. Chem. Miner.*, *30*, 12–19, doi:10.1007/s00269-002-0285-z.

Stolper, E., and S. Newmann (1994), The role of water in the petrogenesis of Mariana trough magmas, *Earth Planet. Sci. Lett.*, *121*, 293–325, doi:10.1016/0012-821X(94)90074-4.

Tenner, T. J., M. M. Hirschmann, A. C. Withers, and R. L. Hervig (2009), Hydrogen partitioning between nominally anhydrous mantle minerals and melt between 3 and 5 GPa and applications to hydrous peridotite partial melting, *Chem. Geol.*, *262*, 42–56, doi:10.1016/j.chemgeo.2008.12.006.

Wallace, P. J., F. A. Frey, D. Weis, and M. F. Coffin (2002), Origin and evolution of the Kerguelen Plateau, Broken Ridge and Kerguelen Archipelago: Editorial, *J. Petrol.*, *43*, 1105–1108, doi:10.1093/petrology/43.7.1105.

Wells, P. R. A. (1977), Pyroxene thermometry in simple and complex systems, *Contrib. Mineral. Petrol.*, *62*, 129–139, doi:10.1007/BF00372872.

Withers, A. C., and M. M. Hirschmann (2007), H_2O storage capacity of $MgSiO_3$ clinoenstatite at 8–13 GPa, 1100–1400°C, *Contrib. Mineral. Petrol.*, *154*, 663–674, doi:10.1007/s00410-007-0215-7.

Withers, A. C., and M. M. Hirschmann (2008), Influence of temperature, composition, silica activity and oxygen fugacity on the H_2O storage capacity of olivine at 8GPa, *Contrib. Mineral. Petrol.*, *156*, 595–605, doi:10.1007/s00410-008-0303-3.

Woodland, A. B., J. Kornprobst, and B. J. Wood (1992), Oxygen thermobarometry of orogenic lherzolite massif, *J. Petrol.*, *22*, 203–230.

Workman, R. K., E. H. Hauri, S. R. Hart, J. H. Wang, and J. Blusztajn (2006), Water and trace element in basaltic glasses from Samoa: Implications for water distribution in the mantle, *Earth Planet. Sci. Lett.*, *241*, 932–951, doi:10.1016/j.epsl.2005.10.028.

Wu, F. Y., R. J. Walker, X. W. Ren, D. Y. Sun, and X. H. Zhou (2003), Osmium isotopic constraints on the age of lithospheric mantle beneath northeastern China, *Chem. Geol.*, *196*, 107–129, doi:10.1016/S0009-2541(02)00409-6.

Wu, F. Y., R. J. Walker, Y. H. Yang, H. L. Yuan, and J. H. Yang (2006), The chemical-temporal evolution of lithospheric mantle underlying the North China Craton, *Geochim. Cosmochim. Acta*, *70*, 5013–5034, doi:10.1016/j.gca.2006.07.014.

Xia, Q. X., X. C. Zhi, Q. Meng, L. Zheng, and Z. C. Peng (2004), The trace element and Re-Os isotopic geochemistry of mantle-derived peridotite xenoliths from Hannuoba: Nature and age of SCLM beneath the area (in Chinese), *Acta Petrol. Sin.*, *20*(5), 1215–1224.

Xu, X. S., S. Y. O'Reilly, W. L. Griffin, X. M. Zhou, and X. L. Huang (1998), The nature of the Cenozoic lithosphere at Nushan, eastern China, in *Mantle Dynamics and Plate Interactions in East China, Geodyn. Ser.*, vol. 27, edited by M. F. J. Flower et al., pp. 167–196, AGU, Washington, D. C.

Xu, X. S., W. L. Griffin, S. Y. O'Reilly, N. J. Pearson, H. Y. Geng, and J. P. Zheng (2008), Re-Os isotopes of sulfides in mantle xenoliths from eastern China: Progress modification of lithospheric mantle, *Lithos*, *102*, 43–64, doi:10.1016/j.lithos.2007.06.010.

Xu, Y. G. (2001), Thermo-tectonic destruction of the Archean lithospheric keel beneath the Sino-Korean craton in China: Evidence, timing and mechanism, *Phys. Chem. Earth A*, *26*, 747–757.

Xu, Y. G., and J. L. Bodinier (2004), Contrasting enrichments in high- and low-temperature mantle xenoliths from Nushan, eastern China: Results of a single metasomatic event during lithospheric accretion?, *J. Petrol.*, *45*, 321–341, doi:10.1093/petrology/egg098.

Xu, Y. G., C. Y. Lin, L. B. Shi, J.-C. C. Mercier, and J. V. Ross (1995), Upper mantle geotherm for eastern China and its geological implications, *Sci. China B*, *38*, 1482–1492.

Xu, Y. G., J. Blusztajn, J. L. Ma, K. Suzuki, J. F. Liu, and S. R. Hart (2008), Late Archean to Early Proterozoic lithospheric mantle beneath the western North China craton: Sr-Nd-Os isotopes of peridotite xenoliths from Yangyan and Fansi, *Lithos*, *102*, 25–42, doi:10.1016/j.lithos.2007.04.005.

Yang, X. Z., Q. K. Xia, E. Deloule, L. Dallai, Q. C. Fan, and M. Feng (2008), Water in minerals of the continental lithospheric mantle and overlying lower crust: A comparative study of peridotite and granulite xenoliths from the North China Craton, *Chem. Geol.*, *256*, 33–45, doi:10.1016/j.chemgeo.2008.07.020.

Ying, J. F., H. F. Zhang, N. Kita, Y. Morishita, and G. Shimoda (2006), Nature and evolution of Late Cretaceous lithospheric mantle beneath the eastern North China Craton: Constraints from petrology and geochemistry of peridotitic xenoliths from Junan, Shandong province, China, *Earth Planet. Sci. Lett.*, *244*, 622–638, doi:10.1016/j.epsl.2006.02.023.

Zhang, H. F. (2005), Transformation of lithospheric mantle through peridotite-melt reaction: A case of Sino-Korean craton, *Earth Planet. Sci. Lett.*, *237*, 768–780, doi:10.1016/j.epsl.2005.06.041.

Zhang, H. F., M. Sun, X. H. Zhou, W. M. Fan, M. G. Zhai, and J. F. Yin (2002), Mesozoic lithosphere destruction beneath the North China Craton: Evidence from major-, trace-element and Sr-Nd-Pb isotope studies of Fangcheng basalts, *Contrib. Mineral. Petrol.*, *144*, 241–253.

Zhang, H. F., S. L. Goldstein, X. H. Zhou, M. Sun, J. P. Zheng, and Y. Cai (2008), Evolution of subcontinental lithospheric mantle beneath eastern China: Re-Os isotopic evidence from mantle xenoliths in Paleozoic kimberlites and Mesozoic basalts, *Contrib. Mineral. Petrol.*, *155*, 271–293, doi:10.1007/s00410-007-0241-5.

Zhang, H. F., S. L. Goldstein, X. H. Zhou, M. Sun, and Y. Cai (2009), Comprehensive refertilization of lithospheric mantle beneath the North China Craton: Further Os-Sr-Nd isotopic constraints, *J. Geol. Soc.*, *166*, 249–259, doi:10.1144/0016-76492007-152.

Zhao, G. C., S. A. Wilde, P. A. Cawood, and M. Sun (2000), Metamorphism of basement rocks in the Central Zone of the North China Craton: Implications for Paleoproterozoic tectonic evolution, *Precambrian Res.*, *103*, 55–88, doi:10.1016/S0301-9268(00)00076-0.

Zhao, G. C., S. A. Wilde, P. A. Cawood, and M. Sun (2001), Archean blocks and their boundaries in the North China Craton: Lithological, geochemical, structural and P-T path constraints and tectonic evolution, *Precambrian Res.*, *107*, 45–73, doi:10.1016/S0301-9268(00)00154-6.

Zheng, J. P., and F. X. Lu (1999), Mantle xenoliths from kimberlites, Shandong and Liaoning: Paleozoic lithospheric mantle character and its heterogeneity (in Chinese), *Acta Petrol. Sin.*, *15*, 65–74.

Zheng, J. P., S. Y. O'Reilly, W. L. Griffin, F. X. Lu, and M. Zhang (1998), Nature and evolution of Cenozoic lithospheric mantle beneath Shandong

Peninsula, Sino-Korea craton, eastern China, *Int. Geol. Rev.*, *40*, 471–499, doi:10.1080/00206819809465220.

Zheng, J. P., S. Y. O'Reilly, W. L. Griffin, F. X. Lu, M. Zhang, and N. J. Person (2001), Relict refractory mantle beneath the eastern North China Block: Significance for lithospheric evolution, *Lithos*, *57*, 43–66, doi:10.1016/S0024-4937(00)00073-6.

Zheng, J. P., W. L. Griffin, S. Y. O'Reilly, J. S. Yang, T. F. Li, M. Zhang, R. Y. Zhang, and J. G. Liou (2006), Mineral chemistry of peridotites from Paleozoic, Mesozoic and Cenozoic lithosphere: Constraints on mantle evolution beneath eastern China, *J. Petrol.*, *47*, 2233–2256, doi:10.1093/petrology/egl042.

Zhi, X. C., L. Reisberg, and X. S. Xu (2007), Re-Os geochemistry of mantle peridotite xenoliths from Nushan (in Chinese), *J. Univ. Sci. Tech. China*, *37*(8), 945–952.

M. Coltorti, Department of Earth Sciences, Ferrara University, Via Saragat 1, I-44100 Ferrara, Italy.

L. Dallai, Istituto di Geoscienze e Georisorse, CNR, sezione di Pisa, Via Moruzzi 1, I-56124 Pisa, Italy.

E. Deloule, Centre de Recherche Pétrographiques et Géochimiques, Centre National de la Recherches Scientifique, rue Nortre Dame Pauvres, BP20, F-54501 Vandoeuvre-lés-Nancy Cedex, France.

M. Feng, Y. Hao, P. Li, Q.-K. Xia, and X. Yang, CAS Key Laboratory of Crust-Mantle Materials and Environments, School of Earth and Space Sciences, University of Science and Technology of China, Hefei 230026, China. (qkxia@ustc.edu.cn)